Cellular automata approach to three-phase traffic theory

2002 J. Phys. A: Math. Gen. 35 9971

(http://iopscience.iop.org/0305-4470/35/47/303)

INSTITUTE OF PHYSICS PUBLISHING JOURNAL OF PHYSICS A: MATHEMATICAL AND GENERAL

J. Phys. A: Math. Gen. **35** (2002) 9971–10013 PII: S0305-4470(02)38672-4

Cellular automata approach to three-phase traffic theory

Boris S Kerner[1], **Sergey L Klenov**[2] **and Dietrich E Wolf**[3]

[1] DaimlerChrysler AG, RIC/TN, HPC: T729, 70546 Stuttgart, Germany
[2] Department of Physics, Moscow Institute of Physics and Technology, 141700 Dolgoprudny, Moscow Region, Russia
[3] Institut für Physik, Gehard-Mercator-Universität Duisburg, D-47048 Duisburg, Germany

Received 25 June 2002
Published 12 November 2002
Online at stacks.iop.org/JPhysA/35/9971

Abstract

The cellular automata (CA) approach to traffic modelling is extended to allow for spatially homogeneous steady state solutions that cover a two-dimensional region in the flow–density plane. Hence these models fulfil a basic postulate of a three-phase traffic theory proposed by Kerner. This is achieved by a synchronization distance, within which a vehicle always tries to adjust its speed to that of the vehicle in front. In the CA models presented, the modelling of the free and safe speeds, the slow-to-start rules as well as some contributions to noise are based on the ideas of the Nagel–Schreckenberg-type modelling. It is shown that the proposed CA models can be very transparent and still reproduce the two main types of congested patterns (the general pattern and the synchronized flow pattern) as well as their dependence on the flows near an on-ramp, in qualitative agreement with the recently developed continuum version of the three-phase traffic theory (Kerner B S and Klenov S L 2002 *J. Phys. A: Math. Gen.* **35** L31). These features are qualitatively different from those in previously considered CA traffic models. The probability of the breakdown phenomenon (i.e. of the phase transition from free flow to synchronized flow) as function of the flow rate to the on-ramp and of the flow rate on the road upstream of the on-ramp is investigated. The capacity drops at the on-ramp which occur due to the formation of different congested patterns are calculated.

PACS numbers: 89.40.+k, 47.54.+r, 64.60.Cn, 64.60.Lx, 05.65.+b, 45.70.Vn

1. Introduction

Traffic on a highway can be either free or congested. In empirical investigations, congested traffic shows a very complex spatial–temporal behaviour (see the reviews [1–4]). Based on a recent empirical study [5, 6] Kerner found out that in congested traffic two different traffic

phases should be distinguished: 'synchronized flow' and 'wide moving jam'. Therefore, there are three traffic phases: (1) free flow, (2) synchronized flow, (3) wide moving jam.

A wide moving jam is a localized structure moving upstream and limited by two fronts where the vehicle speed changes sharply, i.e. within a region that is small compared to the distance between the fronts. A wide moving jam propagates through either free or synchronized flows and through any bottlenecks (e.g. at on-ramps) keeping the velocity of its downstream front [4, 7]. In this respect, it differs from synchronized flow, the downstream front of which is usually *fixed* at the bottleneck, where it occurs. Such *empirical spatial–temporal* features of 'wide moving jams' and 'synchronized flow' are the basis for the distinction of these traffic phases in congested traffic rather than a behaviour of traffic data in the flow–density plane [4, 7, 8].

Wide moving jams do not emerge spontaneously in free flow (with the possible exception that synchronized flow is somehow prohibited [9]). Instead, there is a sequence of two first-order phase transitions [6]: first the transition from free flow to synchronized flow occurs (called the F $\rightarrow$ S transition), and only later and usually at a different location moving jams emerge in the synchronized flow (the S $\rightarrow$ J transition).

Different explanations of these empirical findings have been proposed by various groups in the last few years, but so far they remain controversial (see e.g. [10–26] and the excellent review by Helbing [1]).

1.1. The fundamental diagram approach and cellular automata models of the Nagel–Schreckenberg (NaSch) type

Empirical observations show that the higher the vehicle density is, the lower the average vehicle speed. The average flow rate, which is the product of the average speed and the density, is a function of the density which has a maximum. This curve in the flow–density plane is called the fundamental diagram [1, 2, 27].

Apparently, the empirical fundamental diagram was the reason why already the first traffic flow models [28–32] were based upon the postulate that hypothetical spatially homogeneous and time-independent solutions, where all vehicles have the same distances to their neighbours and move with the same constant speed, (steady state solutions for short) exist that are related to a fundamental diagram, i.e. a curve in the flow–density plane. (Steady state model solutions are often called 'equilibrium' solutions or 'equilibrium' states of a traffic flow model. In this paper, we will use the term 'steady states'.) A subset of these steady states would be unstable with respect to noise or external perturbations. This postulate underlies almost all traffic flow modelling approaches up to now [1, 2] in the sense that the models are constructed such that in the unperturbed, noiseless limit they have a fundamental diagram of steady states, i.e. the steady states form a curve in the flow–density plane.

The congested patterns which are calculated from these models for a homogeneous road (i.e. a road without bottlenecks) [1, 33–35] are due to the instability of steady states of the fundamental diagram within some range of vehicle densities. When perturbed, they decay into a single or a sequence of wide moving jams ('moving clusters' [33]), whose outflows accelerate to rather high speeds comparable to free flow. This is why we find it helpful to classify these models as belonging to what we call the 'fundamental diagram approach'. In section 1.2, another class of models will be described, which belong to the 'three-phase traffic theory' and lead to qualitatively different congested patterns, which are in better agreement with real observations. Its hallmark is a third kind of flow in addition to the wide moving jams and free flow, in which all vehicles interact strongly, but nevertheless drive smoothly at a reduced, rather uniform speed (synchronized flow). In view of the rich phenomenologies

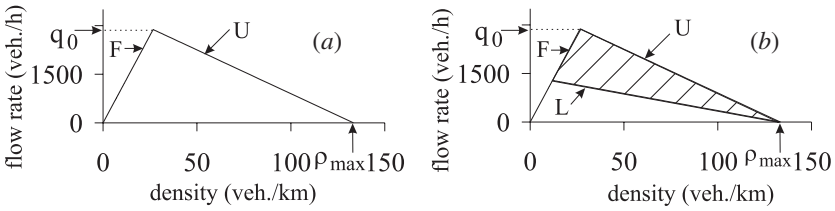

Figure 1. Hypothetical spatially homogeneous and time-independent states (steady states): (*a*) for the initial NaSch CA model [36]; (*b*) the 2D region for the steady states for the KKW-1 model (tables 1 and 3) is the same as in [24].

of the two model classes in particular near an on-ramp, the distinction of the two classes is admittedly a bit simplified at this point, but a more detailed comparison will be given in section 5.

Apart from the congested patterns on a homogeneous road, the dynamical behaviour near an on-ramp differs significantly in the fundamental diagram approach [1, 10–15, 34] and in the three-phase traffic theory [8, 24]. It depends on both the flow rate to the on-ramp q_{on} and the initial flow rate on the road upstream of the on-ramp, q_{in}. Therefore, it can be conveniently characterized by the so-called diagram of congested patterns. This is a map with coordinates q_{on} and q_{in} of the regions, where different congested patterns upstream of the on-ramp occur.

In this paper, we focus on cellular automata (CA) traffic flow modelling which was pioneered by Nagel and Schreckenberg in 1991/1992 [36]. The original Nagel–Schreckenberg (NaSch) model as well as all subsequent modifications and refinements of it [22, 23, 36–39] belong to the fundamental diagram approach (figure 1(*a*)); see also the reviews by Wolf [40], Chowdhury *et al* [2] and Helbing [1]. In this paper, CA models belonging to the three-phase traffic theory will be proposed, and it will be shown that their congested patterns differ qualitatively from those in the CA models of the NaSch type.

Within the fundamental diagram approach, there is a subset of traffic models which show spatially homogeneous high density states with low speed. At first sight these states look like 'synchronized flow', but this interpretation is incompatible with the observed dynamical behaviour near an on-ramp, as will be discussed now. In the diagram of congested patterns near an on-ramp obtained by Helbing *et al* [1, 10] such high density states with low speed occur upstream of the on-ramp, if the flow rate q_{on} to the on-ramp is high enough. Helbing *et al* called these states 'homogeneous congested traffic' (HCT) [10] and proposed to identify it with synchronized flow [1]. In HCT *no* moving jams occur *spontaneously*.

By contrast, in empirical observations of synchronized flow at low vehicle speed and high enough vehicle density moving jams do emerge spontaneously. These moving jams are particularly likely to occur, when due to the high flow rate to the on-ramp a strong compression of synchronized flow appears ('the pinch effect') [6, 8]. In fact, moving jams are *only* observed to emerge spontaneously in synchronized flow upstream of an on-ramp on which the flow rate is high enough [8]. At lower flow rates to the on-ramp synchronized flow of higher vehicle speed can occur in which the nucleation of moving jams was not observed.

1.2. The three-phase traffic theory

To explain the above and other empirical results, Kerner introduced a three-phase traffic theory which postulates that the steady states of synchronized flow cover *a two-dimensional (2D) region* in the flow–density plane, i.e. there is *no* fundamental diagram of traffic flow in this theory [3, 6, 41–43].

This is not excluded by the empirical fact mentioned above, that a given vehicle density determines the *average* vehicle speed. Even if there is a continuous interval of different vehicle speeds at the same distance between vehicles (at the same density), as is indicated by empirical observations of synchronized flow, obviously their averaging leads to one value at the given density. A 2D region of steady states in the flow–density plane is also not ruled out by car-following experiments, where a driver has the task to follow a specific leading car and not to lose contact with it (e.g. [44]). In such a situation, the gap between the cars will be biased towards the security gap depending on the speed of the leading car. In synchronized flow the situation is different: the gap between cars can be much larger than the security gap.

As it has recently been postulated on very general grounds [8, 45] and demonstrated for a microscopic traffic model [24], the fact whether the steady states of a mathematical description of traffic belong to a curve or to a 2D region in the flow–density plane *qualitatively changes* the basic non-linear spatial–temporal features of the congested patterns which the model allows.

In particular, the diagram of the congested patterns at on-ramps is qualitatively different in three-phase traffic theory [8, 24, 45] from the diagram obtained in the fundamental diagram approach [1, 10, 12–15, 17]. Specifically, at a high flow rate to the on-ramp, instead of HCT without moving jams, we find that moving jams always spontaneously emerge in synchronized flow of low vehicle speed and high density, whereas synchronized flow of higher vehicle speed can exist for a long time without an occurrence of moving jams [8, 24, 45]. This agrees with the empirical observations [8].

The microscopic model proposed by Kerner and Klenov in order to derive the diagram of congested patterns within the three-phase traffic theory is relatively complex [24]. The main aim of this paper is a derivation of CA models within the three-phase traffic theory (where steady states of the models cover 2D regions in the flow–density plane) which on the one hand are the most simple ones and on the other hand are able to reproduce the diagram of congested patterns found in [8, 24, 45]. The paper is organized as follows. First, in the next section several CA models with qualitatively different 2D regions in the flow–density plane for steady states will be introduced. Second, the congested patterns at an on-ramp and their diagrams will be numerically derived for these models and compared with one another and with the results in [24]. Third, the probability of the breakdown phenomenon (the F $\rightarrow$ S transition) at an on-ramp is studied and the capacity drop is calculated. Finally, the results of CA models in the three-phase traffic theory and in the fundamental diagram approach are compared.

2. Cellular automata models within three-phase traffic theory

2.1. Equations of motion

The starting point of CA modelling of three-phase traffic theory is the basic set of rules from [24] which provides a 2D region of steady states. Denoting the speed and space coordinates of a vehicle at discrete time $t = n\tau$, $n = 0, 1, 2, \ldots$ by v_n and x_n, respectively, the basic rules are rewritten for CA models in the form

$$v_{n+1} = \max(0, \min(v_{\text{free}}, v_{\text{s},n}, v_{\text{c},n})) \qquad x_{n+1} = x_n + v_{n+1}\tau \tag{1}$$

where v_{free} is the maximum speed of the vehicles. It is assumed to be the same for all vehicles in this paper. $v_{\text{s},n}$ is the safe speed which must not be exceeded in order to avoid collisions. In general it depends on the space gap between vehicles, $g_n = x_{\ell,n} - x_n - d$, and the speed $v_{\ell,n}$ [40, 46], where the lower index ℓ marks functions (or values) related to the vehicle in front of that at x_n, the 'leading vehicle', and d is the vehicle length (assumed to be the same for

all vehicles in this paper). For the sake of comparability we neglect the $v_{\ell,n}$ dependence and choose the same expression as in the standard NaSch model [36]:

$$v_{\mathrm{s},n} = g_n/\tau. \tag{2}$$

The dependence on $v_{\ell,n}$ was included in [24]. It does not change the qualitative features of the congested patterns, but allows, of course, smaller time headways between the vehicles.

The crucial difference compared to previous CA models is that the acceleration behaviour given by $v_{\mathrm{c},n}$ (the rule of 'speed change') depends on whether the leading car is within a 'synchronization distance' $D_n = D(v_n)$ or further away [24]. At sufficiently large distances from the leading vehicle, one simply accelerates with an acceleration a, which is assumed to be the same for all vehicles and independent of time in this paper. However, within the synchronization distance the vehicle tends to adjust its speed to that of the leading vehicle, i.e. it decelerates with deceleration b if it is faster, and accelerates with a if it becomes slower than the leading vehicle. The deceleration b should not be confused with braking for safety purposes (i.e. in order not to exceed $v_{\mathrm{s},n}$). In practice, the speed adjustment within the synchronization distance can often be achieved without braking at all simply as a result of rolling friction of the wheels with the road. Therefore the deceleration b is typically smaller than the braking capability of a vehicle. For simplicity we set $b = a$ in this paper, so that the speed change per time step within the synchronization distance is given by $\Delta v_n = a\tau\ \mathrm{sgn}(v_{\ell,n} - v_n)$, where $\mathrm{sgn}(x)$ is 1 for $x > 0$, 0 for $x = 0$ and -1 for $x < 0$. In summary,

$$v_{\mathrm{c},n} = \begin{cases} v_n + a\tau & \text{for} \quad x_{\ell,n} - x_n > D_n \\ v_n + a\tau\ \mathrm{sgn}(v_{\ell,n} - v_n) & \text{for} \quad x_{\ell,n} - x_n \leqslant D_n. \end{cases} \tag{3}$$

We want to emphasize that this rule decouples speed and gap between vehicles for dense traffic. This can be seen by assuming that vehicles drive behind each other with the same speed v. According to (3) neither the speed nor the gaps will change, provided all the distances are anywhere between the safe distance $d + v\tau$ and the synchronization distance $D(v) \geqslant d + v\tau$. There is neither a speed-dependent distance, which individual drivers prefer, nor is there a distance-dependent optimal speed. This is the principal conceptual difference between three-phase traffic theory and the fundamental diagram approach, and it is the reason why in three-phase traffic theory the steady states fill a 2D region in the flow–density plane, while in the fundamental diagram approach they lie on a curve.

Let us contrast (3) with two models belonging to the fundamental diagram approach, the NaSch model with 'comfortable driving' recently put forward by Knospe *et al* [22, 23, 47] on the one hand, and Wiedemann's modelling approach [48] on the other. Knospe *et al* [22, 23, 47] put forward an extension of the NaSch CA model, in which a driver starts to brake within some interaction horizon, as soon as he sees the brake lights of the vehicle in front being switched on. If nobody puts on the brakes, vehicles would close up to the safe distance, which is a function of the speed. In this sense, the term 'comfortable driving' is a bit misleading: the behaviour modelled is more accurately described as 'comfortable braking'. In contrast, the speed synchronization (3) in our model happens always, whether someone brakes or not. It reflects what we believe to be the typical way, in which drivers take into account the vehicle in front of them.

In Wiedemann's modelling approach [48] each vehicle has a preferred following distance, but convergence to it is hindered due to imperfect perception, so that the actual distance has an oscillatory behaviour. This model also belongs to the fundamental diagram approach, as the steady state solutions have a unique relationship between speed and distance between vehicles.

Of course, in models with a fundamental diagram of steady states, fluctuations and external perturbations let the system evolve in time through a 2D region in the flow–density plane as well. However, the dynamics is governed locally by steady state properties, the unstable

steady states acting as 'repellers' and the stable ones as 'attractors'. If the steady states form a 2D region, part of which is stable and part of which is metastable, as is the case in three-phase traffic theory, the dynamics is fundamentally different. This leads also to qualitative differences between the patterns of congested traffic obtained in three-phase traffic theory or in the fundamental diagram approach, respectively, as will be shown in detail below.

2.2. Synchronization distance

Conditions (1) and (3) are the basis of the CA models under consideration. It will be shown that this allows different formulations for fluctuations, acceleration, deceleration and for the synchronization distance D_n which all lead to qualitatively the same features of congested patterns and the same diagram of these patterns as postulated in three-phase traffic theory [8, 45] and in agreement with the continuum model of Kerner and Klenov in [24].

In particular, let us consider two different formulations for the dependence of the synchronization distance D_n on the vehicle speed. In the first formulation, the synchronization distance D_n in (3) is a linear function of the vehicle speed:

$$D(v_n) = d_1 + kv_n\tau. \tag{4}$$

In the second formulation, the synchronization distance D_n in (3) is a non-linear function of the vehicle speed:

$$D(v_n) = d + v_n\tau + \beta v_n^2 \big/ 2a. \tag{5}$$

In (4) and (5) d_1, k and β are positive constants. Both formulations lead to 2D regions of steady states in the flow–density plane.

2.3. Steady states

Whereas in models belonging to the fundamental diagram approach (e.g. [10, 12, 16, 18, 22, 23, 36, 39, 46, 47, 49] and the reviews [1, 2]) a vehicle would close up to the leading one adjusting its speed and gap as required by secure driving, in models with the basic structure (1), (3), a driver within the synchronization distance D_n adapts his speed to that of the vehicle in front without caring what the precise gap is, as long as it is safe. This explains why there is no unique flow–density relationship for steady states in the present CA models.

In steady states all accelerations must be zero. Then the time index n can be dropped in the above formulae. According to (1)–(3), there are two possibilities: either the synchronization distance $D(v) < g + d$ and the speed is $v = v_{\text{free}}$, or

$$D(v) \geqslant g + d \quad \text{and} \quad v = v_\ell \leqslant \min(v_{\text{free}}, v_s(g, v)). \tag{6}$$

Thus, in steady states all speeds are equal v. The conditions v has to fulfil are only equal if also the gaps g are all equal. Therefore, we defined steady states above as time independent and homogeneous.

The density ρ and the flow rate q are related to the gap g and the speed v by

$$\rho = 1/(x_\ell - x) = 1/(g + d) \qquad q = \rho v = v/(g + d). \tag{7}$$

Because v and g are integer in CA models, the steady states do not form a continuum in the flow–density plane as they do in [24]. However, the inequalities of (6) define a 2D region in the flow–density plane, in which steady states exist. As in [24] it is limited by three boundaries (figure 1(*b*) and figures 2(*a*) and (*b*)), the upper line U, the lower curve L and the left line F. The parameters of the lines F and U are chosen to be the same for all CA models under consideration. Note that without the lower boundary L, the lines F and U constitute the fundamental diagram of the NaSch CA model (figure 1(*a*)) [36].

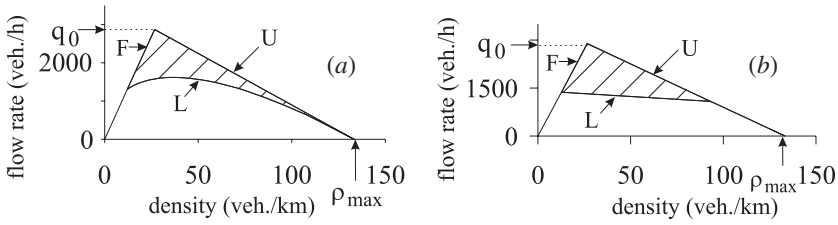

Figure 2. 2D regions supporting steady states in the flow–density plane for two of the KKW models (tables 1 and 3): (*a*) for KKW-2 model (non-linear dependence of the synchronization distance (5) on the vehicle speed); (*b*) for KKW-4 model (linear synchronization distance (4) with $d_1 < d$).

The left boundary F is given by $q = \rho v_{\text{free}}$. This is free flow, where the flow rate q is not restricted by safety requirements. On the upper boundary U the flow rate is determined by the safe speed v_{s}. For example, inserting (2) and (7) it is given by

$$q = \rho v_{\text{s}} = (1 - \rho d)/\tau. \tag{8}$$

The lower boundary L is determined by the synchronization distance D: a steady state with density ρ and a speed $v < v_{\text{free}}$ requires that $D(v) \geqslant 1/\rho$ with equality on the lower boundary L. For example, using (4) with $d_1 = d$ one obtains (see figure 1(*b*))

$$q = (1 - \rho d)/k\tau. \tag{9}$$

In the second model (5) the lower boundary L is a non-linear curve (see figure 2(*a*)):

$$q = \frac{\tilde{\rho}}{\tau}\left(\sqrt{1 + \frac{2}{\tilde{\rho}}(1 - \rho d)} - 1\right) \qquad \text{with} \quad \tilde{\rho} = \frac{\rho\tau^2 a}{\beta}. \tag{10}$$

This curve has the upper line U as a tangent at $\rho = \rho_{\max} = 1/d$. As will be shown below, this allows us to reproduce qualitatively the diagram of congested patterns of three-phase traffic theory with simpler fluctuations than what is needed in the case of the linear synchronization distance (4) with $d_1 = d$. However, if the parameter d_1 is chosen smaller than d in (4), the line L intersects the line U before the jam density $\rho_{\max}$ is reached (figure 2(*b*)). In this case, if the difference $d - d_1$ is chosen in a proper way, the fluctuations in the model with linear synchronization distance (4) may be as simple as for the non-linear D (5), in order to lead to qualitatively the same features. We also did simulations (not shown in this paper), where we replaced d in (5) by $d_1 < d$; the qualitative results remain unchanged.

2.4. Fluctuations of acceleration and deceleration

In order to show the power of the basic model (1), (3) [24], the remaining model specifications (free and safe speeds, fluctuations) will be the same as introduced in different NaSch CA models in the fundamental diagram approach [22, 23, 36, 38, 39, 49, 50] (with a slightly more general modelling of fluctuations). Nevertheless, it will be shown that all features of congested patterns which spontaneously occur upstream of the on-ramp as well as of their evolution (when the flow rate to the on-ramp is changing) are different in our CA models. This proves that the basic rules (1), (3) [24] place our CA models in the class belonging to the three-phase traffic theory.

In particular, as in the NaSch CA models [22, 23, 36, 38, 39, 49], the accelerations and decelerations are stochastic. They are implemented like in [22, 39]. *In the first step*, a

preliminary vehicle speed of each vehicle $\tilde{v}_{n+1}$ is

$$\tilde{v}_{n+1} = v_{n+1} \tag{11}$$

where v_{n+1} is calculated based on the system of the dynamical equations (1)–(3). *In the second step*, a fluctuation $a\tau\eta_n$ (to be specified below) is added to the value $\tilde{v}_{n+1}$ calculated from the first step. *Finally*, the speed v_{n+1} at the time $n+1$ is calculated by

$$v_{n+1} = \max(0, \min(\tilde{v}_{n+1} + a\tau\eta_n, v_n + a\tau, v_{\text{free}}, v_{\text{s},n})). \tag{12}$$

This means that the stochastic contribution $a\tau\eta_n$ may neither lead to a speed smaller than zero, nor to a speed larger than what the deterministic acceleration a would give, taking the limitations by v_{free} and $v_{\text{s},n}$ into account.

We implement the fluctuation η_n in (12) as

$$\eta_n = \begin{cases} -1 & \text{if} \quad r < p_{\text{b}} \\ 1 & \text{if} \quad p_{\text{b}} \leqslant r < p_{\text{b}} + p_{\text{a}} \\ 0 & \text{otherwise} \end{cases} \tag{13}$$

where r denotes a random number uniformly distributed between 0 and 1. This is a generalization of the random deceleration (with probability p_{b}) in NaSch CA automata models [22, 23], because with probability p_{a} also a random acceleration can occur. $p_{\text{a}} + p_{\text{b}} \leqslant 1$ must be fulfilled. In a different way and for a different purpose, a random acceleration was also introduced in CA models by Brilon and Wu [50]. As in a NaSch CA model in the fundamental diagram approach [39], the probability p_{b} in (13) is taken as a decreasing function of the vehicle speed v_n:

$$p_{\text{b}}(v_n) = \begin{cases} p_0 & \text{if} \quad v_n = 0 \\ p & \text{if} \quad v_n > 0 \end{cases} \tag{14}$$

where p and $p_0 > p$ are constants. This corresponds to the slow-to-start rules first introduced by Takayasu and Takayasu [51] and later used in the NaSch CA model by Barlovic *et al* [39]: vehicles escape at the downstream front of a wide moving jam with the mean delay time $\tau_{\text{del}} = \tau/(1-p_0)$. As in [23] this provides the jam propagation through free and synchronized flows with the same velocity v_{g} of the downstream jam front that corresponds to a qualitative theory and to the related formula $v_{\text{g}} = -1/(\rho_{\max}\tau_{\text{del}})$ from [6]. $\rho_{\max} = 1/d$ is the density inside the jam.

The probability p_{a} of the random acceleration in (13) is also taken as a decreasing function of the vehicle speed v_n,

$$p_{\text{a}}(v_n) = \begin{cases} p_{\text{a1}} & \text{if} \quad v_n < v_{\text{p}} \\ p_{\text{a2}} & \text{if} \quad v_n \geqslant v_{\text{p}}. \end{cases} \tag{15}$$

where v_{p}, p_{a1} and $p_{\text{a2}} < p_{\text{a1}}$ are constants. This simulates the effect that the vehicle moving at low speed in the dense flow tends to close up to the leading one. Indeed, according to (1)–(4), (12) and (13), if the probability p_{a} of the acceleration is high, the effect of adapting one's speed to the speed of the leading vehicle is weak: with probability p_{a} the vehicle does not reduce its speed, and it may do so until it reaches the minimal safe gap. Note that the tendency to minimize the space gap at low speed can lead in particular to the 'pinch' effect in synchronized traffic flow [4, 6], i.e. to the self-compression of the synchronized flow at lower vehicle speed with the spontaneous emergence of moving jams.

The tendency to minimize the space gap at low speed is automatically built into our models, if the lower boundary L approaches the upper line U as in figure 2(*a*) and (*b*), because then the synchronization distance is no longer larger than the security gap at small speed. Indeed, it turns out that the speed dependence (15) of p_{a} is not required in these cases for a

realistic modelling. Therefore, we choose the probability p_a of acceleration in (13) to be a constant in the model variants of figure 2.

2.5. Cellular automata models with cruise control within three-phase traffic theory

Nagel and Paczuski [37] proposed a variant of the NaSch CA model where fluctuations are turned off for the vehicle speed $v_n = v_{free}$. This variant has been called the NaSch CA model with *cruise control* [1, 37].

In the case of such cruise control, i.e. when fluctuations are turned off for the vehicle speed $v_n = v_{free}$, simpler CA models can be used, if either the synchronization distance is the non-linear one, (5) (figure 2(*a*)), or in the synchronization distance (4) $d_1 < d$ (figure 2(*b*)).

In these cases, the CA models with cruise control within three-phase traffic theory consist again of formulas (1)–(3) and (5) (or (4) where $d_1 < d$). The formula (12) for the incorporation of fluctuations into the final value of the speed v_{n+1} at time $(n+1)\tau$ is also valid, but can be simplified, if only deceleration noise like in the NaSch-type CA [22, 23, 39] is implemented,

$$\eta_n = \begin{cases} -1 & \text{if} \quad r < p_b \\ 0 & \text{otherwise} \end{cases} \tag{16}$$

with the probability [37, 39]

$$p_b(v_n) = \begin{cases} p_0 & \text{if} \quad v_n = 0 \\ p & \text{if} \quad 0 < v_n < v_{free} \\ 0 & \text{if} \quad v_n = v_{free}. \end{cases} \tag{17}$$

Then $\tilde{v}_{n+1} + a\tau\eta_n \leqslant \tilde{v}_{n+1}$ so that (12) can also be written in the simpler form

$$v_{n+1} = \max(0, \tilde{v}_{n+1} + a\tau\eta_n). \tag{18}$$

2.6. Summary of the new models and their parameters

In the following sections, we shall discuss the congestion patterns obtained from simulations of four CA models belonging to the class of three-phase traffic theory as introduced above. For easier reference, we specify them in table 1 with the abbreviations KKW-1 to KKW-4. In addition, we provide two tables containing a list of symbols (table 2) and typical values for the parameters (table 3).

A few remarks on the time and space discretization are in order. The usual choice of the time step τ in CA models of traffic is $\tau = 1$ s [2, 36]. As in [22] we use a small-scale discretization of space: the length of cells is chosen equal to $\delta x = 0.5$ m. This leads to a speed discretization in units of $\delta v = 1.8$ km h^{-1}. Hence, two vehicles are only considered as moving with different speeds if this difference is equal to (or larger than) δv. In the model [24] with continuous changes in the vehicle speed, two vehicle speeds are considered to be different, if their difference exceeds a much smaller value $\delta v = 10^{-6}$ m s^{-1}. This is one of the reasons why fluctuations in CA automata are in general stronger than in the corresponding continuum model.

For all CA models within the three-phase traffic theory investigated here, we chose the probability $p_0 = 0.425$. This corresponds to a velocity $v_g = -15.5$ km h^{-1} of the downstream front of a wide moving jam and an outflow $q_{out} = 1810$ vehicles/h from a wide moving jam. Note that the flow rate q_{out} refers to the case where the vehicles reach the maximum vehicle speed $v = v_{free}$, after they have escaped from the jam.

For the sake of comparison with other traffic models, we choose occasionally in section 5 model parameters deviating from those given in table 3. In this case, the parameter values are given in the related figure captions.

Table 1. Definition of four CA models KKW-1–KKW-4.

Dynamical part of all KKW models

$$\tilde{v}_{n+1} = \max(0, \min(v_{\text{free}}, v_{\text{s},n}, v_{\text{c},n})) \qquad g_n = x_{\ell,n} - x_n - d$$

$$v_{\text{s},n} = g_n/\tau \qquad v_{\text{c},n} = \begin{cases} v_n + a\tau & \text{for} \quad g_n > D_n - d \\ v_n + a\tau\ \text{sgn}(v_{\ell,n} - v_n) & \text{for} \quad g_n \leqslant D_n - d \end{cases}$$

v_{free}, d, τ and a are constants

Stochastical part of all KKW models

$$v_{n+1} = \max(0, \min(\tilde{v}_{n+1} + a\tau\eta_n, v_n + a\tau, v_{\text{free}}, v_{\text{s},n})) \qquad x_{n+1} = x_n + v_{n+1}\tau$$

$$\eta_n = \begin{cases} -1 & \text{if} \quad r < p_{\text{b}} \\ 1 & \text{if} \quad p_{\text{b}} \leqslant r < p_{\text{b}} + p_{\text{a}} \\ 0 & \text{otherwise} \end{cases}$$

Specifications of synchronization distance D_n and noise η_n

For CA model KKW-1 (cf figure 1(*b*))

$$D_n = d + kv_n\tau \qquad p_{\text{b}}(v_n) = \begin{cases} p_0 & \text{if} \quad v_n = 0 \\ p & \text{if} \quad v_n > 0 \end{cases} \qquad p_{\text{a}}(v_n) = \begin{cases} p_{\text{a1}} & \text{if} \quad v_n < v_{\text{p}} \\ p_{\text{a2}} & \text{if} \quad v_n \geqslant v_{\text{p}} \end{cases}$$

constant parameters: k, p_0, p, p_{a1}, p_{a2}, v_{p}

For CA model KKW-2 (cf figure 2(*a*))

$$D_n = d + v_n\tau + \beta v_n^2 \big/ 2a, \qquad p_{\text{b}}(v_n) = \begin{cases} p_0 & \text{if} \quad v_n = 0 \\ p & \text{if} \quad v_n > 0 \end{cases}$$

constant parameters: β, p_0, p, p_{a}

For CA model KKW-3 (cf figure 2(*a*))

$$D_n = d + v_n\tau + \beta v_n^2 \big/ 2a \qquad p_{\text{b}}(v_n) = \begin{cases} p_0 & \text{if} \quad v_n = 0 \\ p & \text{if} \quad 0 < v_n < v_{\text{free}} \\ 0 & \text{if} \quad v_n = v_{\text{free}} \end{cases}$$

constant parameters: $p_{\text{a}} = 0$, β, p_0, p

For CA model KKW-4 (cf figure 2(*b*)):

$$D_n = d_1 + kv_n\tau \qquad p_{\text{b}}(v_n) = \begin{cases} p_0 & \text{if} \quad v_n = 0 \\ p & \text{if} \quad v_n > 0 \end{cases}$$

constant parameters: $d_1 < d$, k, p_0, p, p_{a}

3. Congested patterns on a homogeneous one-lane road

All CA models introduced here (table 1) show qualitatively similar results on the homogeneous one-lane road. Therefore, only numerical results of a simulation of model KKW-1 (figure 1(*b*)) will be presented in this section.

For simulations of congested patterns on a homogeneous one-lane road, cyclic boundary conditions have been used. The one-lane homogeneous road has the length 60 000 cells (30 km). We checked that all qualitative results remain the same, if open boundary conditions are used and the length of the road is large enough.

3.1. Complex dynamics of synchronized flow

The features of spatiotemporal pattern formation on a homogeneous road (i.e. a road without bottlenecks or on-ramps) are largely the same for the KKW models considered here and the continuum model of Kerner and Klenov [24]. However, due to stronger fluctuations in the CA models, the dynamics of perturbations is somewhat different.

(i) If the initial flow rate q_{in} does not exceed a value $q_{\max} < q_0$,

$$0 < q_{\text{in}} < q_{\max} \tag{19}$$

Table 2. List of symbols.

τ	time discretization interval
δx	space discretization length
$\delta v = \delta x/\tau$	speed discretization unit
$n = 0, 1, 2, \ldots$	number of time steps
$\tilde{v}_n$	vehicle speed at time step n without fluctuating part
v_n	vehicle speed at time step n
$v_{\ell,n}$	speed of the leading vehicle at time step n
$v_{\mathrm{s},n}$	safe speed at time step n
v_{free}	maximal speed (free flow)
x_n	vehicle position at the time step n
$x_{\ell,n}$	position of the leading vehicle at time step n
d	vehicle length
$g_n = x_{\ell,n} - x_n - d$	gap (front to end distance) at time step n
D_n	synchronization distance at time step n
a	vehicle acceleration
b	vehicle deceleration
η_n	speed fluctuation at time step n
p_{a}	probability of vehicle acceleration
p_{b}	probability of vehicle deceleration
r	random number uniformly distributed between 0 and 1
q_0	maximum flow rate in steady states
$q_{\max}$	maximum flow rate in free flow ($v = v_{\mathrm{free}}$)
$\rho_{\max} = 1/d$	density of traffic jam
v_{g}	velocity of downstream front of wide moving jam
q_{out}	flow rate in the outflow from a wide moving jam
$\rho_{\min}$	density in free flow related to the flow rate q_{out}
t_0	time at which vehicle influx from on-ramp is switched on
$q_{\mathrm{lim}}^{(\mathrm{pinch})}$	limit flow rate in pinch region of general pattern
$q_{\mathrm{out}}^{(\mathrm{bottle})}$	outflow from a congestion pattern at an on-ramp

the fluctuations do not perturb the speed of a vehicle, which initially has maximal speed v_{free}, significantly (figures 3(a)–(c)). In this case, the fluctuations lead to changes in the distances between vehicles, i.e. to a change in the vehicle density and hence to a change in the flow rate (black points F in figure 3(c)).

(ii) However, if

$$q_{\max} \leqslant q_{\mathrm{in}} \leqslant q_0 \tag{20}$$

the model fluctuations lead to an occurrence of inhomogeneous and non-stationary synchronized flow states where the vehicle speed is lower than v_{free} (figures 3(d)–(f)). According to Kerner's hypothesis about continuous spatiotemporal transitions between different states of synchronized flow in three-phase traffic theory [41–43] this behaviour corresponds to a complex motion within the 2D region in the flow–density plane, where steady states exist (open circles S in figure 3(f)). Similar continuous spatiotemporal transitions between different states of synchronized flow in agreement with Kerner's hypothesis have recently also been found in a different CA model by Fukui *et al* [26].

These inhomogeneous synchronized flow states are the result of many independent local transitions at different road locations. As they cause a reduction of the initial maximal vehicle speed, they look similar to the F $\rightarrow$ S transitions on the two-lane road which have been studied in [24]. However, in [24] the F $\rightarrow$ S transition was in general caused by an external

Table 3. Model parameters and characteristic values.

Common parameters and values for all KKW models	
Discretization units	$\tau = 1$ s, $\delta x = 0.5$ m, $\delta v = \delta x/\tau = 1.8$ km h^{-1}, $a = \delta v/\tau = 0.5$ m s^{-2}
Model parameters	$v_{\text{free}} = 108$ km h$^{-1} = 60\,\delta v$, $d = 7.5$ m $= 15\,\delta x$, $p_0 = 0.425$
Model results	$v_{\text{g}} = -15.5$ km h^{-1}, $q_{\text{out}} = 1810$ vehicles/h, $\rho_{\min} = 16.76$ vehicles/km, $q_0 = 2880$ vehicles/h
CA model KKW-1	
General model parameters	$k = 2.55$, $v_{\text{p}} = 50.4$ km h$^{-1} = 28\delta v$, $p_{\text{a1}} = 0.2$
Parameter-set I:	
model parameters	$p = 0.04$, $p_{\text{a2}} = 0.052$
model results	$q_{\max} \approx 2400$ vehicles/h, $q_{\text{lim}}^{(\text{pinch})} \approx 1150$ vehicles/h
Parameter-set II:	
model parameters	$p = 0.055$, $p_{\text{a2}} = 0.085$
model results	$q_{\max} \approx 2630$ vehicles/h, $q_{\text{lim}}^{(\text{pinch})} \approx 1000$ vehicles/h
CA model KKW-2	
Model parameters	$p = 0.04$, $p_{\text{a}} = 0.052$, $\beta = 0.05$
Model results	$q_{\max} \approx 2400$ vehicles/h, $q_{\text{lim}}^{(\text{pinch})} \approx 1150$ vehicles/h
CA model KKW-3	
Model parameters	$p = 0.04$, $\beta = 0.05$
Model results	$q_{\max} \approx 1460$ vehicles/h, $q_{\text{lim}}^{(\text{pinch})} \approx 1150$ vehicles/h
CA model KKW-4	
Model parameters	$d_1 = 2.5$ m $= 5\,\delta x$, $k = 2.55$, $p = 0.04$, $p_{\text{a}} = 0.052$

local perturbation, which led to the formation of a local region of synchronized flow (see figure 1(c) in [24]). By contrast, in the CA models under consideration the local transitions were induced by the intrinsic model fluctuations in a wide range of densities given by (20). No external local perturbation was applied. As a consequence, a complex inhomogeneous spatiotemporal pattern of synchronized flow appears everywhere on the road instead of the local region triggered by a perturbation in the continuum model (compare figure 3(d) in this paper with figure 1(c) in [24]).

(iii) A homogeneous initial state with vehicle speed lower than v_{free}, which in the absence of fluctuations would belong to the steady states within the 2D region of the flow–density plane, remains a synchronized flow state for a long time. However, as in (ii) the evolution of these synchronized flow states shows a complex spatiotemporal behaviour of all traffic flow variables (figure 4) due to the intrinsic model fluctuations.

3.2. Emergence of wide moving jams

The emergence of wide moving jams (figure 5) shows qualitatively the same features as in [24].

(i) In particular, as in [24], moving jams do *not* occur spontaneously if the initial state with maximal vehicle speed $v = v_{\text{free}}$ lies within the range of flow rates (19), where the maximal speed can be maintained.

For a subset of these states, those with a density above a threshold for the wide moving jam formation, $\rho_{\min}$ (figures 3(c) and (f) and figure 5(c)), wide moving jams can be induced, but only by a very strong local perturbation. For the case when traffic flow with the maximal

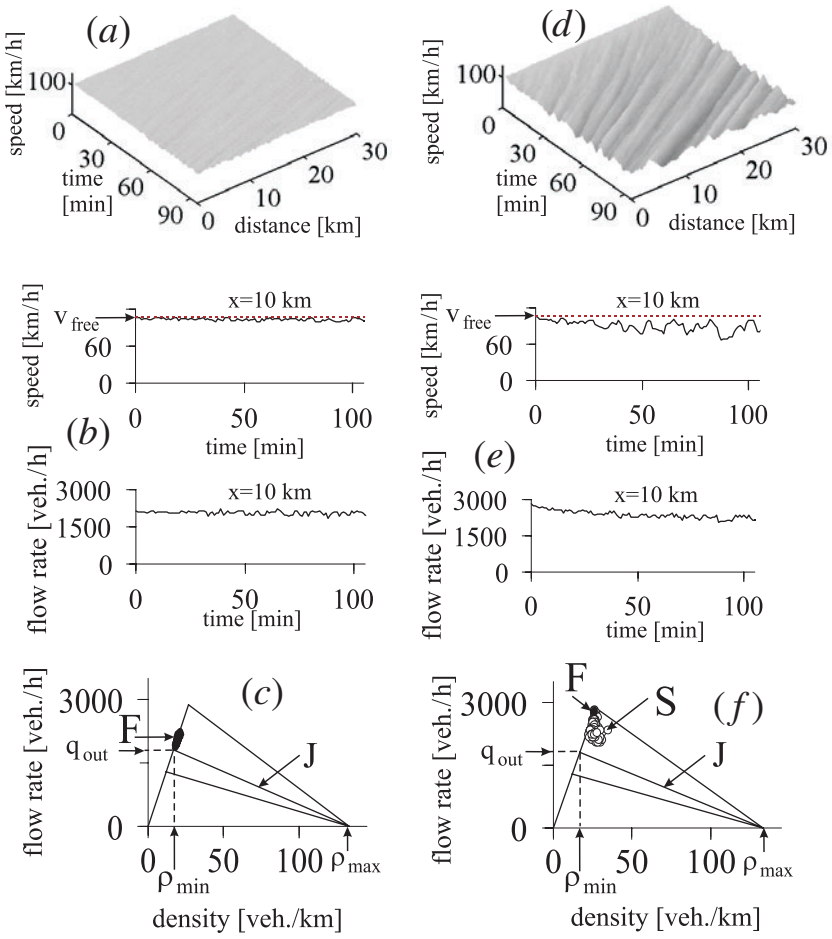

Figure 3. Traffic patterns on a homogeneous one-lane road with periodic boundary conditions for KKW-1 model (parameter-set I of table 3). (a, b, c) Perturbation of free flow at moderate flow rate ($q = 2160$ vehicles/h $< q_{\max} \approx 2400$ vehicles/h) and (d, e, f) at high flow rate ($q = 2842$ vehicles/h $> q_{\max}$). (a, d) Vehicle speed as function of time and distance (distance increases in downstream direction); (b, e) vehicle speed and flow rate at the location $x = 10$ km as functions of time (one minute averaged data of virtual detectors); (c, f) data in the flow–density plane which correspond to (b, e), respectively.

vehicle speed $v = v_{\text{free}}$ is formed downstream of a wide moving jam, the density $\rho_{\min}$ is related to the flow rate in the outflow of the wide moving jam, q_{out}.

The velocity of the downstream front of the wide moving jam v_{g} is a characteristic, i.e. unique, predictable and reproducible parameter which is a constant for given model parameters. This velocity together with the threshold point, $(\rho_{\min}, q_{\text{out}})$, determines the characteristic line J for the downstream front of a wide moving jam (the line J in figures 3(c) and (f), figures 4(c) and 5(c)).

The strength of the perturbation needed to trigger a wide moving jam is highest for densities close to $\rho_{\min}$. Then it is not enough that a vehicle is forced to stop (the maximal amplitude of a perturbation), but this stop must be maintained for some time (about 2–3 minutes at $\rho_{\min}$) for a wide moving jam to nucleate in an initial traffic flow with maximal speed $v = v_{\text{free}}$. Note that for initial densities which are only slightly higher than $\rho_{\min}$ a wide

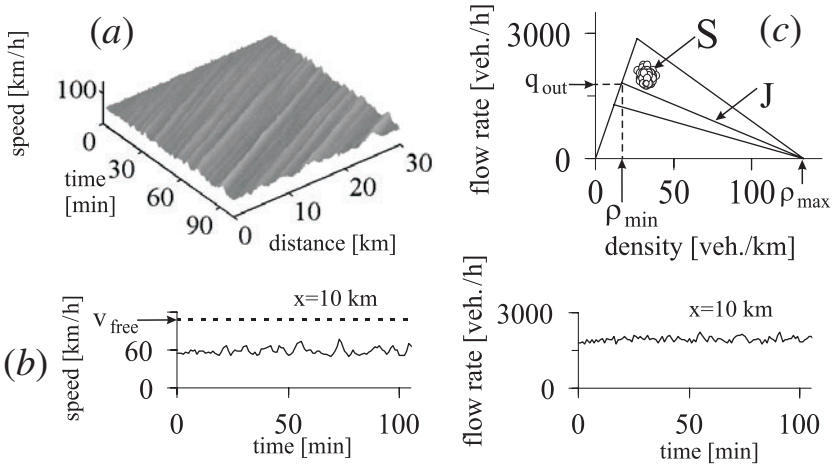

Figure 4. Synchronized flow behaviour on a homogeneous one-lane road with periodic boundary conditions for KKW-1 model (parameter-set I of table 3). (*a*) Vehicle speed as a function of time and distance; (*b*) vehicle speed (left) and flow rate (right) at a fixed location ($x = 10$ km) as functions of time (one minute averages); (*c*) data in the flow–density plane which correspond to (*b*). Initial free flow $q_{\rm in} = 1800$ vehicles/h, initial speed $v_{\rm in} = 54$ km h^{-1} ($v_{\rm in} = 15$ m s^{-1}).

moving jam often spontaneously disappears due to the high fluctuations of the outflow from the jam in the KKW-1 model.

(ii) As in [24], the line J determines the threshold of the wide moving jam excitation in synchronized flow: all densities in steady synchronized flows related to the line J are threshold densities with respect to the jam formation (the S $\rightarrow$ J transition). At a given speed, the higher the density, the lower is the critical amplitude $\delta v_{\rm c}$ of a local perturbation for the S $\rightarrow$ J transition: the critical amplitude $\delta v_{\rm c}$ for the S $\rightarrow$ J transition reaches its maximum value at the threshold density. At a given difference between an initial density and the threshold density, the lower the initial speed, the lower the critical amplitude $\delta v_{\rm c}$ is.

However, for synchronized flow states which lie in the vicinity of the safe speed (in the vicinity of the line U in figures 1(*b*) and 2) the strong intrinsic model fluctuations in the KKW models (table 1) lead to the S $\rightarrow$ J transition without the need of any external local perturbation.

(iii) The latter result allows a simulation of the spontaneous emergence of wide moving jams (figures 5(*a*)–(*c*)). In the initial state, all vehicles move with the maximal speed $v = v_{\rm free}$. For a flow rate in the interval (20), the initial vehicle speed $v = v_{\rm free}$ cannot be maintained for a long time: due to local transitions, the vehicle speed decreases and states of synchronized flow are formed at some locations on the road (figures 5(*b*) and (*c*) at $x = 14$ km) as already described in (ii) in section 3.1. In these synchronized flow states, model fluctuations grow leading to the *spontaneous* emergence of wide moving jam (figures 5(*a*), (*b*) and (*c*) at $x = 8$ km). For the model parameters used in figure 5 the spontaneous emergence of a wide moving jam can also occur for an initial state of synchronized flow with speed $v_{\rm in} < v_{\rm free}$.

Note that the fluctuation parameters p and $p_{\rm a2}$ of both random deceleration and random acceleration are larger than in figures 3 and 4, where no spontaneous emergence of wide moving jams from synchronized flow states was observed within the simulation time. Fast drivers are more 'nervous' in figure 5 than in the previous figures. However, this is not the only reason for the emergence of wide moving jams in the present example. This can be seen by comparing the average values of the random contribution η to the speed for speeds larger than

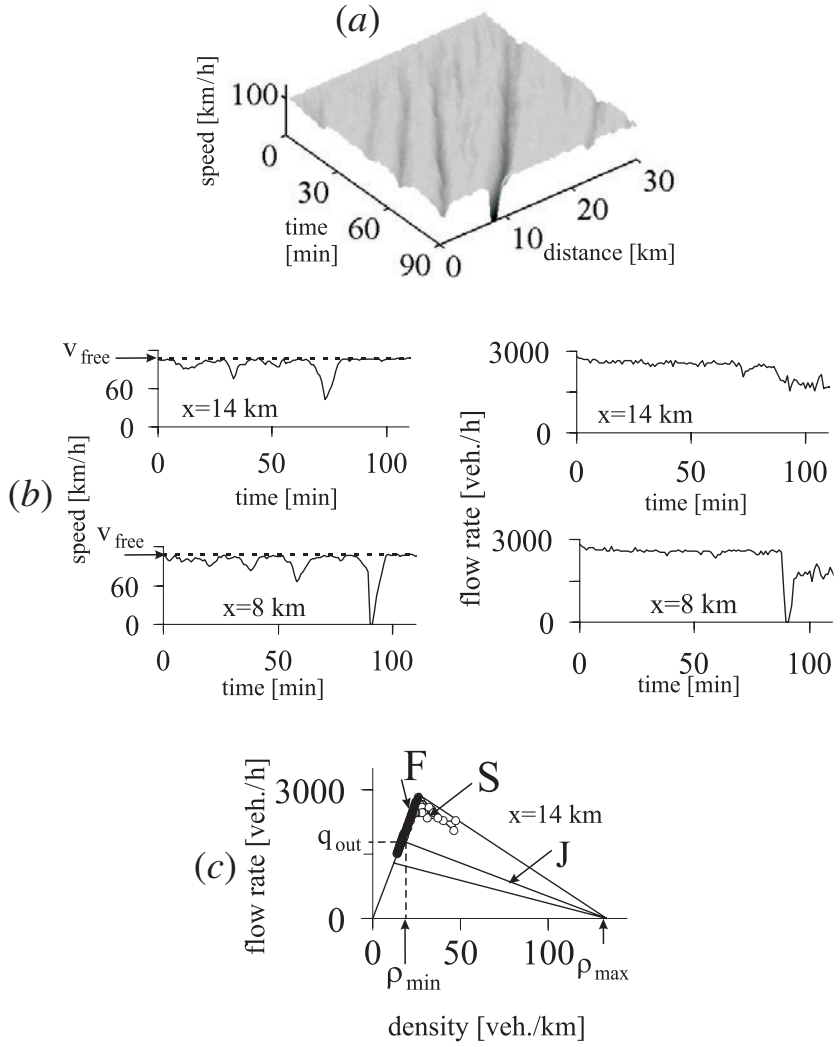

Figure 5. Wide moving jam formation on a homogeneous one-lane road with periodic boundary conditions for KKW-1 model with parameter-set II of table 3, where the probabilities of random deceleration, p, and random acceleration at high speed, p_{a2}, are larger than in figure 3. (*a*) Vehicle speed as function of time and distance; (*b*) vehicle speed and flow rate at the locations $x = 14$ km and $x = 8$ km as functions of time (one minute averages); (*c*) data in the flow–density plane which correspond to (*b*) at the location $x = 14$ km. Initial free flow rate $q_{\rm in} = 2842$ vehicles/h is larger than $q_{\rm max} \approx 2630$ vehicles/h (cf (19) and (20)). In (*c*) black points are related to the states of free flow with speed v close to $v_{\rm free}$ (the points *F*), and circles are related to states of synchronized flow (the points *S*).

$v_{\rm p} = 50.4$ km h^{-1}: while in the previous figures $\langle\eta\rangle = p_{\rm a2} - p = 0.012$, it is here more than twice as large, $\langle\eta\rangle = 0.03$. A positive value of $\langle\eta\rangle$ means that the drivers are biased towards stochastic acceleration rather than deceleration. A stronger bias implies a higher delay time in the vehicle deceleration. We will come back to the question how this makes wide moving jams more likely, below, in section 4.2(ii).

(iv) Thus, as in the model of Kerner and Klenov [24], in an initial traffic flow with the maximal speed $v = v_{\rm free}$ model fluctuations can cause the spontaneous occurrence of

synchronized flow, but not the spontaneous emergence of wide moving jams. The latter was only found in the KKW models (table 1), once synchronized flow was established. That synchronized flow states should occur first and only later the spontaneous wide moving jam, is a common feature of three-phase traffic theory and agrees with empirical observations [3, 6]. Thus, in the KKW models within the three-phase traffic theory the diagram of congested patterns on the homogeneous road is qualitatively different from those in other approaches [1, 2].

4. Congested patterns at on-ramps

4.1. Model of on-ramp

In this section, for all simulations of congested patterns at an on-ramp a one-lane road of 100 km length (200 000 cells) with open boundary conditions is used. The reference point $x = 0$ is placed at the distance 20 km from the end of the road, so that it begins at the coordinate $x = -80$ km. The on-ramp starts at the point $x = 16$ km (32 000 cells) and its merging area was 0.3 km long (600 cells).

For simulation of the on-ramp, two consecutive vehicles on the main road within the on-ramp area are chosen randomly, their coordinates being denoted by $x^+ > x^-$. The entering vehicle is placed in the middle point between them at the coordinate $x_n = [(x^+ + x^- + 1)/2]$ (here [ ] denotes the integer part), taking the speed of the leading vehicle v^+ [18]. In addition, it was required that the distance between the two vehicles on the main road should exceed some value

$$dx_{\mathrm{on}}^{(\min)} = \lambda v^+ + 2d \tag{21}$$

where λ was chosen to be equal to 0.55, if not stated explicitly otherwise.

Our numerical investigations have shown that the main qualitative features of congested patterns at the on-ramp and of the related diagrams do not change, if instead of these simple rules for a vehicle squeezing in from the on-ramp to the road more sophisticated lane-changing rules are used. It is important, however, that on the one hand the model of the on-ramp allows a gradual change of the flow rate to the on-ramp q_{on} from nearly zero to a relatively large (but for traffic flow relevant) value, and on the other hand does not introduce large additional speed fluctuations, when a vehicle from the on-ramp merges with the traffic flow on the main road.

4.2. Diagrams of congested patterns at on-ramps

A diagram of congested patterns at the on-ramp represents regions of spontaneous occurrence of congested patterns upstream of the on-ramp at different values of the initial flow rate to the on-ramp q_{on} and the initial flow rate on the one-lane road q_{in} upstream of the on-ramp. As will be discussed in more detail below, these regions in principle depend on how long one waits, i.e. on how far one samples rare events. In practice, a typical waiting time much longer than one hour has little meaning, as real traffic is not a stationary stochastic process on large time scales.

We found that the CA models under consideration (table 1) essentially show the same diagram of congested patterns which has been predicted for the three-phase traffic theory [8] and previously obtained in the continuous microscopic model [24]. However, for some parameter values there are interesting peculiarities in the KKW models.

(i) In figures 6(*a*) and (*b*) the diagram of congested patterns at an on-ramp is shown for two different sets of the parameters-of the KKW-1 model (table 1) (parameter-set I and parameter-set II in table 3, respectively). Although the KKW-1 model is considerably simpler

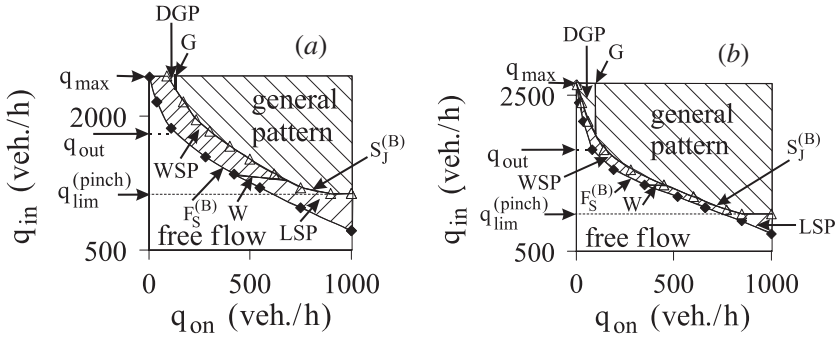

Figure 6. Diagrams of congested patterns at the on-ramp for the KKW-1 model. (*a*) Parameter-set I of table 3 as in figure 3. (*b*) Parameter-set II of table 3 as in figure 5. GP—general pattern, DGP—dissolving general pattern, WSP—widening synchronized flow pattern and LSP—localized synchronized flow pattern.

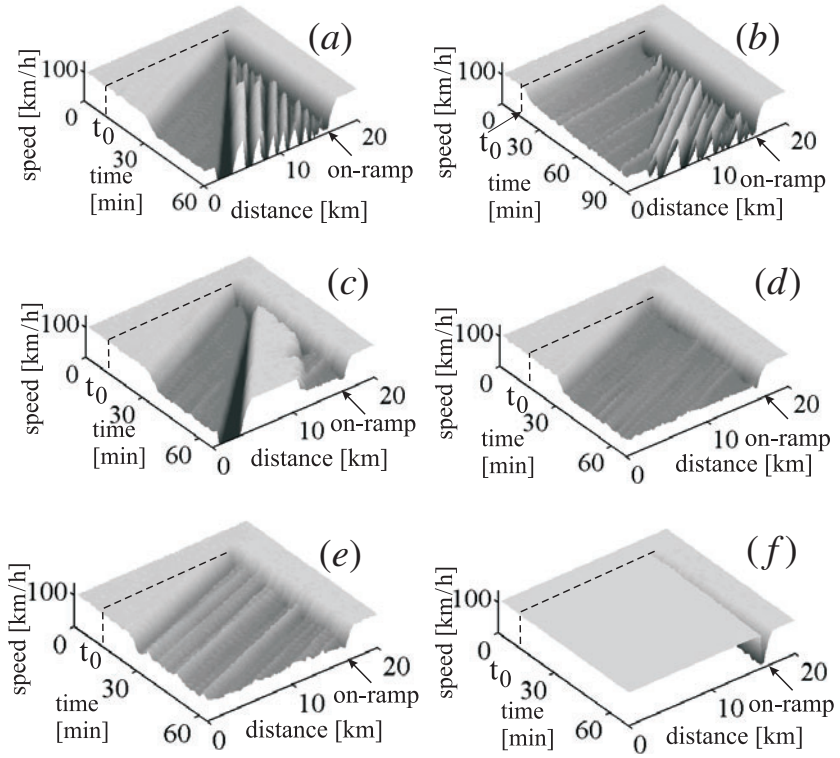

Figure 7. Congested patterns at the on-ramp belonging to figure 6(*a*). (*a*) General pattern (GP) at $q_{in} > q_{out}$, (*b*) GP at $q_{in} < q_{out}$, (*c*) dissolving general pattern (DGP), (*d*, *e*) widening synchronized flow patterns (WSP) and (*f*) localized synchronized flow pattern (LSP). At $t_0 = 8$ min flow from the on-ramp is switched on. Single vehicle data are averaged over a space interval of 40 m and a time interval of 1 min. The flow rates (q_{on}, q_{in}) are: (*a*) (500, 2300), (*b*) (740, 1740), (*c*) (105, 2400), (*d*) (90, 2300), (*e*) (90, 2160), and (*f*) (760, 1080) vehicles/h.

than the model of Kerner and Klenov studied in [24], the main features of the diagram (figure 6(*a*)) and the related congested patterns which spontaneously occur upstream of the on-ramp (figures 7, 8 and 9) are qualitatively the same as in [24].

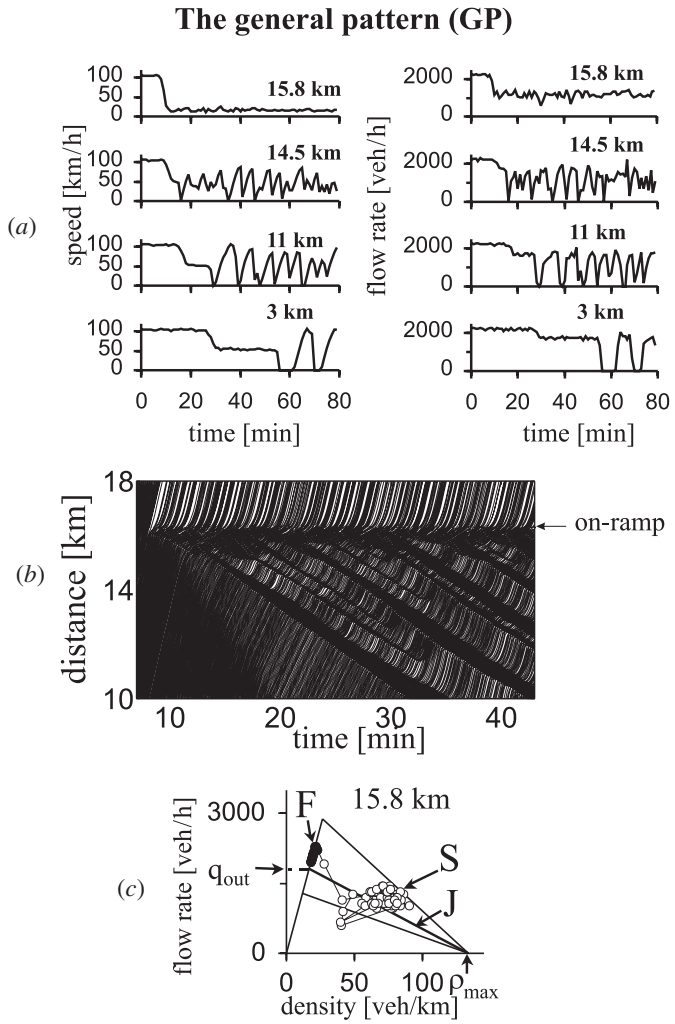

Figure 8. The general pattern (GP) (KKW-1 model parameters as in figure 7(*a*)): (*a*) vehicle speed (left) and flow rate (right), (*b*) vehicle trajectories, (*c*) the corresponding data in the flow–density plane for the location $x = 15.8$ km. (*a*, *c*) One minute averaged data of virtual detectors whose coordinates are indicated in the related figures. In (*c*) black points are related to the states of free flow with the speed v close to the maximal one v_{free} (the points *F*) and circles are related to states of synchronized flow (the points *S*). To show the spatiotemporal features of the GP clearly, only trajectories of every 6th vehicle are shown in (*b*).The dashed line in (*b*) shows the upstream front of the pattern which separates synchronized flow downstream from free flow upstream.

There are two main boundaries $F_S^{(B)}$ and $S_J^{(B)}$ on the diagram (figure 6). The limit point of the boundary $F_S^{(B)}$ at $q_{\text{on}} \to 0$ is related to the maximum flow rate in free flow at the on-ramp where $q_{\text{in}} = q_{\max}$.

Below and left of the boundary $F_S^{(B)}$ free flow occurs. Between the boundaries $F_S^{(B)}$ and $S_J^{(B)}$ different synchronized flow patterns (SP) occur upstream of the on-ramp, without wide moving jams being observed.

Right of the boundary $S_J^{(B)}$ wide moving jams spontaneously emerge in synchronized flow which has been formed upstream of the on-ramp. The only difference compared to the results

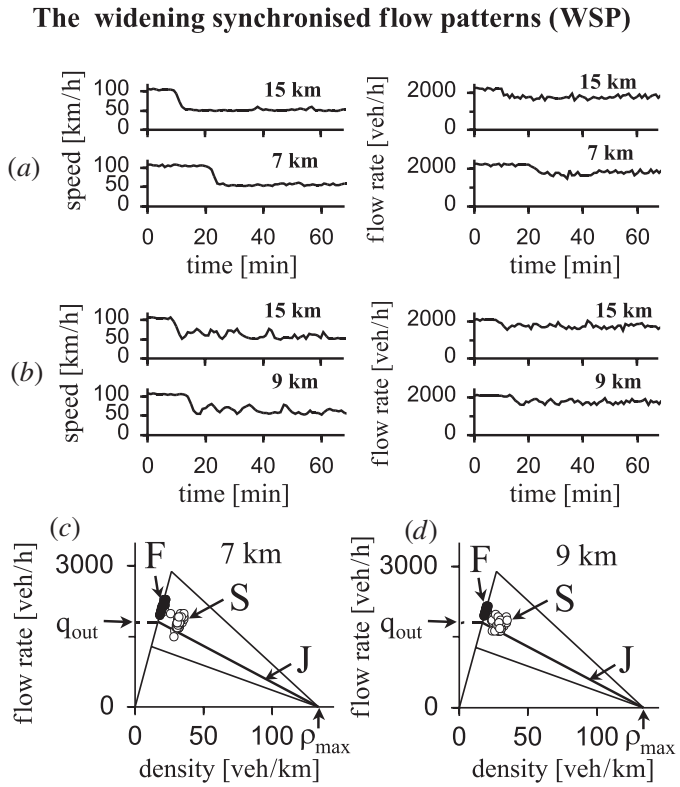

Figure 9. The widening synchronized flow pattern (WSP): (*a*) the vehicle speed (left) and the flow rate (right), (*c*) the corresponding data on the flow–density plane for WSP shown in figure 7(*d*). The similar plots (*b*), (*d*) are for WSP shown in figure 7(*e*). One minute averaged data of virtual detectors whose coordinates are indicated in (*a*–*d*). In (*c*), (*d*) black points are related to the states of free flow with the speed v close to the maximal one $v_{\rm free}$ (the points F) and circles are related to states of synchronized flow (the points S). The KKW-1 model parameters for (*a*, *c*) are the same as in figure 7(*d*) and for (*b*, *d*) as in figure 7(*e*).

in [24] is that in figure 6(*a*) there is no region where the moving synchronized flow pattern (MSP) occurs (about a possible occurrence of MSP see below). The diagram in figure 6(*a*) is in accordance with general features of the diagrams of congested patterns at the on-ramp on a one-lane road which was postulated from qualitative considerations in [8].

A few technical remarks about the determination of the boundary $F_S^{(B)}$ are in order: after the on-ramp has been switched on at $t = t_0$, there is a transient, before the congested patterns are established upstream of the on-ramp, and one needs some criterion to detect the transition from free to synchronized flow. The criterion we used is that the speed drops below some threshold value $V_{\rm FS}$ and stays low for at least 4 min. The value of $V_{\rm FS}$ is chosen equal to 80 km h^{-1}.

The delay time, until this criterion of the transition from free flow to synchronized flow is fulfilled, is marked as $T_{\rm FS}$ in figure 10. This delay time can be rather short ($\approx$1–2 min) for large values of $q_{\rm on}$ (figure 10(*a*)) and increases for decreasing $q_{\rm on}$ (figure 10(*b*)). For small values of $q_{\rm on}$ the speed returns quickly to high values, whenever it happens to drop below $V_{\rm FS}$. Then one would not speak of a transition into synchronized flow any more (figure 10(*c*)). This behaviour of $T_{\rm FS}$ has been used to determine the boundary $F_S^{(B)}$. Scanning the ($q_{\rm on}$, $q_{\rm in}$)-plane

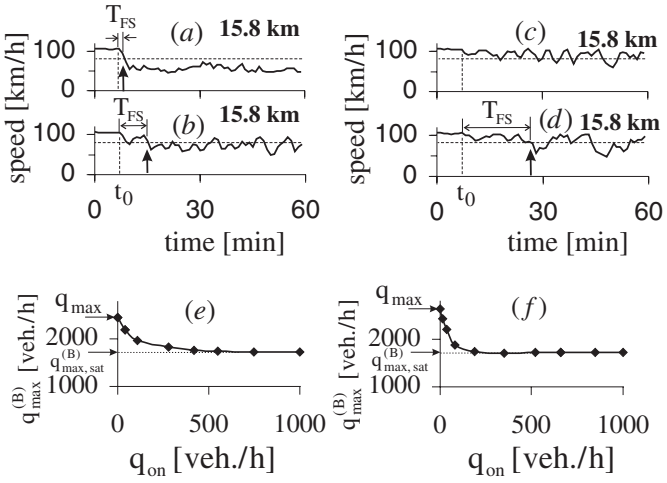

Figure 10. Speed breakdown due to the F → S transition at the location $x = 15.8$ km (0.2 km upstream of the beginning of the on-ramp). Fixed flow rate $q_{\text{in}} = 2000$ vehicles/h. Flow rate q_{on} is: (*a*) 120, (*b*) 90, (*c*) 55 and (*d*) 70 vehicles/h. Up-arrows mark the time $t_0 + T_{\text{FS}}$, at which according to our criterion synchronized flow is detected: the vehicle speed drops below the level 80 km h^{-1} (dashed horizontal line) and remains low for more than 4 min. Simulations of the KKW-1 model (parameter-set I of table 3). In (*e*, *f*) the dependences of the maximal highway capacity in free flow at the on-ramp, $q^{(B)}_{\text{max}}$, on the flow rate to theon-ramp q_{on} are shown. They are related to the boundary $F_S^{(B)}$ in figures 6(*a*) and (*b*), respectively for (*e*) and (*f*).

on a grid the leftmost points were determined, where T_{FS} is still smaller or equal to 30 min in a substantial fraction of independent simulation runs (more than 36 out of 40 realizations) (cf *section 4.5*) (figure 10(*d*)). Similarly, a point on the boundary $S_J^{(B)}$ is found as the leftmost point (q_{on}, q_{in}), where a wide moving jam emerges in synchronized flow within 60 min. Thus, the quantitative positions of the boundaries $F_S^{(B)}$ and $S_J^{(B)}$ depend on the chosen time intervals and the fraction of realizations which show the transitions. However, the qualitative forms of these boundaries are independent of the choice of the time intervals, provided they are high enough.

(ii) The diagram of congested patterns at the on-ramp in figure 6(*b*) is obtained for the same model KKW-1 (table 1) as in (*a*), however with the fluctuation (parameters parameter-set II in table 3). As pointed out already in connection with figure 5, this means that the delay time of vehicle deceleration was increased compared to figure 6(*a*). This has two effects: first, the region between the boundaries $F_S^{(B)}$ and $S_J^{(B)}$, where SP occur without spontaneous wide moving jam formation, is reduced. Second, the boundaries $F_S^{(B)}$ and $S_J^{(B)}$ merge in the limit point $q_{\text{in}} = q_{\text{max}}$, where $q_{\text{on}} \to 0$. This means that in the CA model with higher delay time of vehicle deceleration wide moving jams can spontaneously occur in synchronized flow already at extremely low flow rates to the on-ramp in the vicinity of the point $q_{\text{in}} = q_{\text{max}}$.

This can be explained by realizing that in the present model, an increase in the delay time of vehicle deceleration makes the effect of speed adjustment within the synchronization distance weaker. As a result, it becomes more likely that a vehicle closes up to the leading one, i.e. reaches the minimal safe gap g_n, so that model fluctuations more easily get amplified to cause a wide moving jam.

The F → S transition occurs at the on-ramp during a given time interval T_{FS}, if the flow rates q_{on} and q_{in} correspond to points on the boundary $F_S^{(B)}$ (figure 6). Corresponding to a

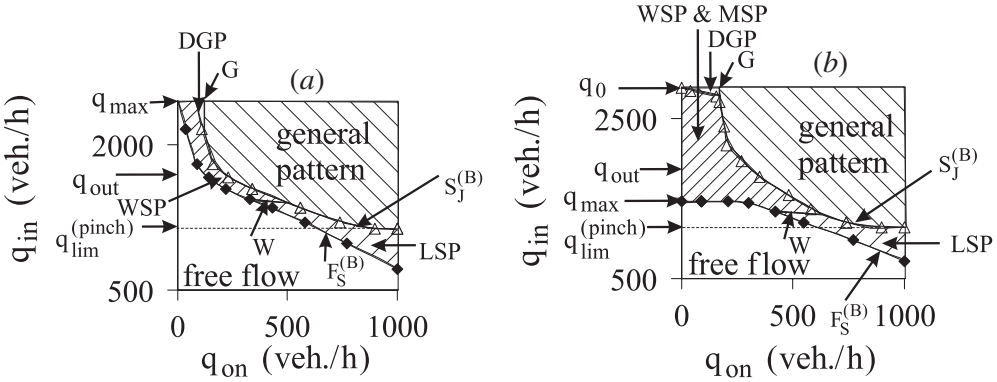

Figure 11. Diagrams of congested patterns at the on-ramp for the KKW-models with non-linear dependence of the synchronization distance (5) on the vehicle speed (figure 2(*a*)): (*a*) KKW-2 model, (*b*) KKW-3 model (tables 1 and 3). GP—general pattern, DGP—dissolving general pattern, WSP—widening synchronized flow pattern, MSP—moving synchronized flow pattern and LSP—localized synchronized flow pattern. Note that for the KKW-2 model (*a*) and the KKW-3 model (*b*) the value V_{FS} discussed in section 4.2(i) is also chosen equal to 80 km h^{-1}. However for the KKW-3 model there is the exception for the case, when q_{in} is close to the point of intersection of the curves L and F (figure 2(*a*)). Near this point the minimal speed in WSP can be greater than 80 km h^{-1}, and the threshold speed V_{FS} is chosen as the average between v_{free} and this minimal speed.

theory of highway capacity following from Kerner's three-phase traffic theory [52] there is an infinite multitude of maximal highway capacities in free flow at the on-ramp $q_{\mathrm{max}}^{(B)}$ which are related to different flow rates $q_{\mathrm{sum}} = q_{\mathrm{on}} + q_{\mathrm{in}}$ at the boundary $F_S^{(B)}$:

$$q_{\mathrm{max}}^{(B)} = q_{\mathrm{sum}}|_{F_S^{(B)}}. \tag{22}$$

The higher the q_{on}, the lower is the maximal capacity $q_{\mathrm{max}}^{(B)}$ (figures 10(*e*) and (*f*)). However there can be a saturation of the decrease in $q_{\mathrm{max}}^{(B)}$ (figure 10(*e*) and (*f*)): the maximal capacity does not reduce below some value $q_{\mathrm{max,sat}}^{(B)}$ even at a very high flow rate to the on-ramp q_{on}. The maximal capacity is highest at $q_{\mathrm{on}} \to 0$:

$$q_{\mathrm{max}}^{(B)}|_{q_{\mathrm{on}}\to 0} = q_{\mathrm{max}}. \tag{23}$$

(iii) In model KKW-2 (non-linear synchronization distance $D(v)$) the diagram of congested patterns at the on-ramp (figure 11(*a*)) and the related congested patterns upstream of the on-ramp (figures 12–14) possess the same qualitative features as shown in figure 6.

There is a peculiarity of the diagram of congested patterns (figure 11(*b*)) for model KKW-3 (cruise control). In this case, there are no model fluctuations at the maximal speed $v = v_{\mathrm{free}}$. Thus, if the flow rate to the on-ramp $q_{\mathrm{on}} = 0$ and the initial state is related to the maximal speed $v = v_{\mathrm{free}}$, synchronized flow with lower vehicle speed cannot appear *spontaneously* up to the top flow rate $q_{\mathrm{in}} = q_0$ (see figures 11(*b*) and 2(*a*)).

However, already at an extremely low flow rate of $q_{\mathrm{on}} \approx$ 1–2 vehicles/h these synchronized flow states with lower speed spontaneously appear upstream of the on-ramp, because of a small disturbance of the initial flow at the on-ramp. Moreover, the flow rate $q_{\mathrm{in}} = q_{\mathrm{max}}$ at which this effect occurs can be noticeably lower than q_{out} in this case (figure 11(*b*)). Therefore, at all flow rates q_{in} within the range

$$q_{\mathrm{max}} \leqslant q_{\mathrm{in}} \leqslant q_0. \tag{24}$$

SP occur spontaneously at the on-ramp for q_{on} as small as 1–2 vehicles/h (figure 11(*b*)).

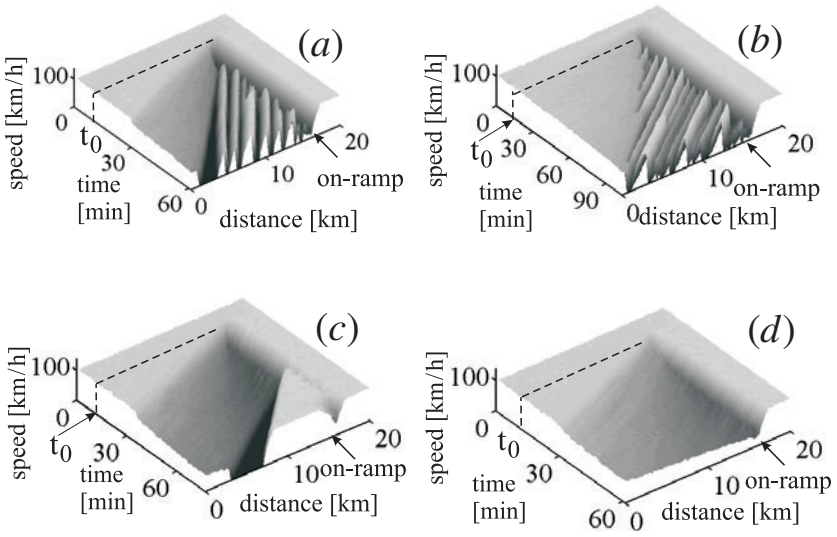

Figure 12. Congested patterns at the on-ramp for the KKW-2 model of figure 11(*a*): (*a*) general pattern (GP) at $q_{\text{in}} > q_{\text{out}}$, (*b*) GP at $q_{\text{in}} < q_{\text{out}}$, (*c*) dissolving general pattern (DGP), (*d*) widening synchronized flow pattern (WSP). Single vehicle data are averaged over a space interval of 40 m and a time interval of 1 min; $t_0 = 8$ min. The flow rates (q_{on}, q_{in}) are: (*a*) (500, 2250), (*b*) (800, 1650), (*c*) (110, 2400) and (*d*) (70, 2300) vehicles/h.

We found that the KKW-4 model, which differs from KKW-2 only by having the synchronization distance which leads to figure 2(*b*) rather than figure 2(*a*), can show qualitatively the same diagram of congested patterns as obtained for model KKW-2 (figure 11(*a*)). Likewise, if one replaces the non-linear synchronization distance in the cruise control model KKW-3 by formula (4) with $d_1 < d$ (as in KKW-4), the diagram of congested patterns can remain qualitatively the same as figure 11(*b*).

To explain these results, first recall that in all these KKW models the probability p_{a} (15) was independent of the vehicle speed, in contrast to the previously considered KKW-1 model. The fact that this simplification of acceleration noise nevertheless allows us to simulate the qualitatively correct pattern formation in the three-phase traffic theory, can be traced back to the difference in the 2D regions of the steady states in the flow–density plane for these CA models.

For *low vehicle speeds* the boundary L for these models is either tangential to the boundary U (figure 2(*a*)), or even coincides with it (figure 2(*b*)). On the other hand, the numerical study of the KKW models shows that, if the vehicle speed in synchronized flow is very close to the safe speed, i.e. for synchronized states close to the boundary U, fluctuations easily lead to the emergence of a wide moving jam. As already mentioned, the purpose of introducing acceleration noise in our models is a simulation of the pinch effect, where moving jams emerge spontaneously. Both models in figure 2 are sufficiently sensitive to fluctuations at low speeds that the pinch effect can be achieved with a relatively small probability p_{a} independent of the vehicle speed.

In contrast, in the KKW-1 model the boundary L of the 2D region of steady states is not close enough to the boundary U even at low vehicle speeds (figure 1(*b*)). In particular, there are synchronized states with low vehicle speed, which lie below the line J. Therefore, the probability p_{a} had to be chosen higher at low speeds in order to enhance the likelihood that a driver comes close to the boundary U. Then the pinch effect is also obtained in this model, in accordance with empirical observations in [6, 8].

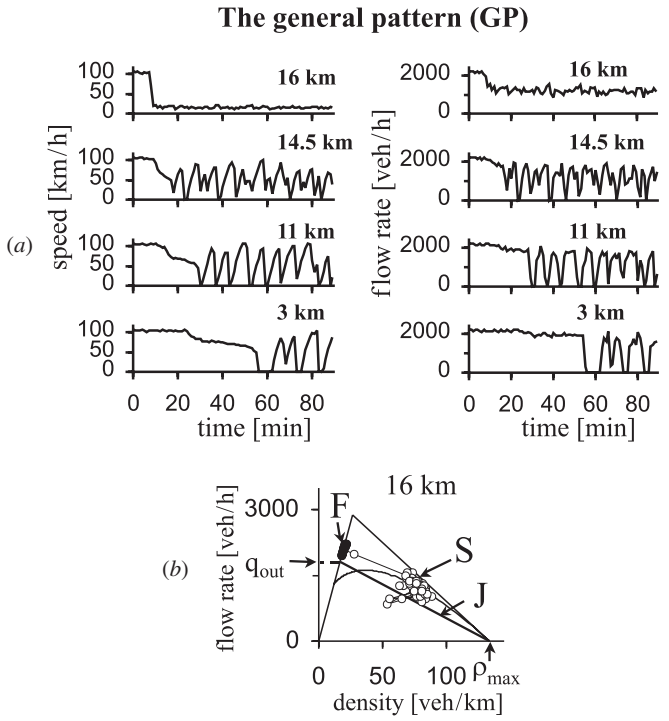

Figure 13. The general pattern (GP) related to figure 12(*a*) (KKW-2 model): (*a*) vehicle speed (left) and flow rate (right), (*b*) corresponding data in the flow–density plane at the location $x = 16$ km. One minute averaged data of virtual detectors, whose coordinates are indicated in (*a*, *b*). In (*b*) black points are related to the states of free flow with the speed v close to the maximal one v_{free} (the points *F*) and circles are relatedto states of synchronized flow (the points *S*).

4.3. Synchronized flow patterns (SP)

As in [24], depending on the parameters either the widening synchronized flow pattern (WSP), or the moving synchronized flow pattern (MSP), or the localized synchronized flow pattern (LSP) can occur in our CA models.

(i) As in [24], WSP occurs at high initial flow rate on the road upstream of the on-ramp, q_{in}, and low flow rate to the on-ramp, q_{on}, between the boundaries $F_S^{(B)}$ and $S_J^{(B)}$. The downstream front of WSP is localized at the on-ramp. The upstream front is continuously moving upstream, so that the width of WSP is gradually increasing in time (figures 7(*d*) and (*e*), figures 9(*a*) and (*b*) and figures 12(*d*), 14, 15(*b*) and 16)).

(ii) Depending on the flow rates q_{in} and q_{on} the distribution of the vehicle speeds inside WSP can be related to states with nearly homogeneous speed (figure 7(*d*) and figures 9(*a*) and (*c*)), or to non-homogeneous speed distributions, where sometimes non-stationary vehicle speed waves (propagating with different, negative and positive velocities) can occur (figure 7(*e*) and figures 9(*b*) and (*d*)).

(iii) Note a peculiarity of the KKW models: the upstream front in WSP which separates synchronized flow downstream and free flow upstream moves with a relatively high velocity $\left(v_{\text{g}}^{(\text{WSP})} \approx -40 \text{ km h}^{-1}\right)$. This non-realistic velocity is a consequence of simplicity of the models presented. In spite of this, the models give a realistic qualitative description of congested patterns and their evolution. More correct values for the front velocity have been found in the microscopic model of Kerner and Klenov [24]. The other way to obtain realistic

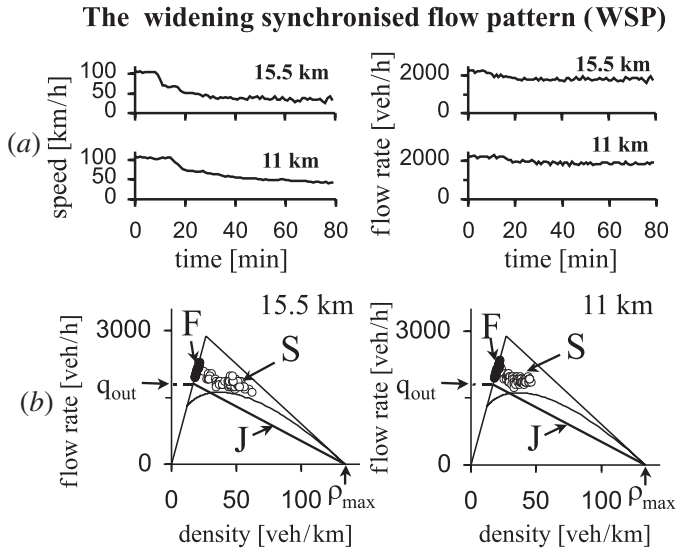

Figure 14. The widening synchronized flow pattern (WSP) related to figure 12 (*d*) (KKW-2 model): (*a*) vehicle speed (left) and flow rate (right), (*b*) the corresponding data on the flow–density plane. One minute averaged data of virtual detectors, whose coordinates are indicated in (*a*, *b*). In (*b*) black points are related to the states of free flow with thespeed v close to the maximal one v_{free} (the points *F*) and circles are related to states of synchronized flow (the points *S*).

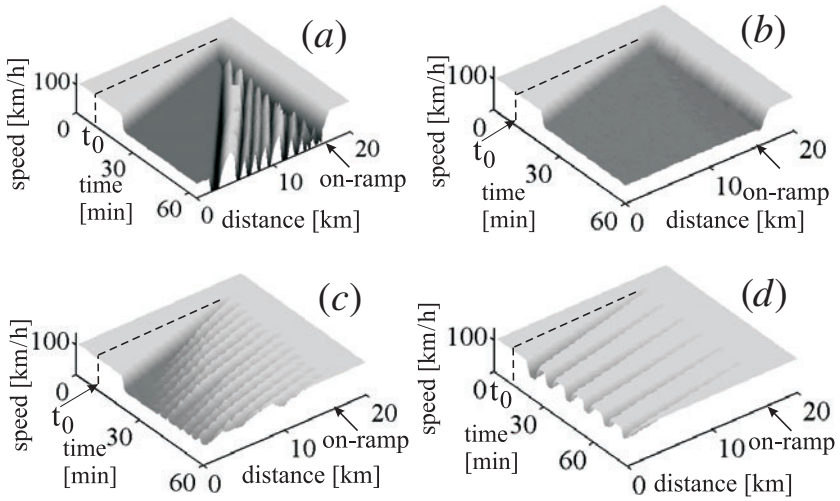

Figure 15. Congested patterns at the on-ramp for the KKW-3 model of figure 11(*b*): (*a*) general pattern (GP), (*b*) widening synchronized flow pattern (WSP), (*c*) widening synchronized flow pattern (WSP) at a lower value of the flow rate to the on-ramp than in (*b*) and (*d*) moving synchronized flow pattern (MSP). Single vehicle data are averaged over a space interval of 40 m and a time interval of 1 min; $t_0 = 8$ min. The flow rates (q_{on}, q_{in}) are: (*a*) (480, 2300), (*b*) (120, 2160), (*c*) (15, 2160) and (*d*) (5, 2040) vehicles/h.

velocity of the front between free and synchronized flows may be the use of a strongly non-uniform free flow upstream of the on-ramp. In this case, there is a large spread of gaps between vehicles in free flow. As a result, the speed of the front is diminished due to the presence of vehicles with too small gaps between them.

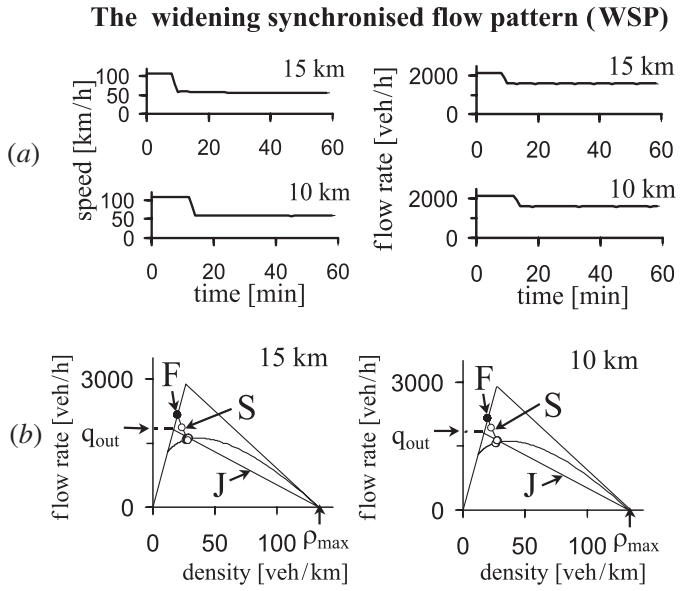

Figure 16. The widening synchronized flow pattern (WSP) related to figure 15(*b*) (KKW-3 model): (*a*) vehicle speed (left) and flow rate (right), (*b*) the corresponding data on the flow–density plane. One minute averaged data of virtual detectors, whose coordinates are indicated in (*a*, *b*).

(iv) Recall that at very low flow rate to the on-ramp, q_{on}, and high initial flow rate on the road upstream of the on-ramp, q_{in}, in the diagram derived in [24] there is a region 'MSP', where the MSP spontaneously occurs. In this case, after SP has emerged upstream of the on-ramp, this SP comes off the on-ramp and begins to move upstream. In some cases, a new SP emerges at the on-ramp; this SP comes off the on-ramp later, and so on.

In contrast to the diagram of congested patterns in [24], WSP can appear also at very low flow rate to the on-ramp q_{on} (figures 6 and 11). In other words, there is no region 'MSP' in our diagrams which looks like that postulated by Kerner [8] based on a qualitative consideration of the three-phase traffic theory approach for a one-lane road. However, in [8] it was also mentioned that fluctuations may cause MSP in the region, where WSP exists normally. Apparently for this reason, sometimes MSP appears at very low flow rate to the on-ramp q_{on} (close to the boundary $F_S^{(B)}$) in the region of WSP in the CA models.

This effect is shown for the KKW-3 cruise control model (table 1) in figures 15(*d*) and 17, where MSP usually occurs in the region marked 'WSP & MSP' in the related diagram of congested patterns (figure 11(*b*)) at lower flow rate to the on-ramp, q_{on}. Within the region 'WSP & MSP' (at a slightly higher flow rate q_{on} than that at which MSP occurs) a pattern which looks like a mixture of WSP and MSP can occur (figure 15(*c*)); near the on-ramp this pattern resembles MSP. However, upstream of the on-ramp the pattern transforms more and more into WSP. Note another peculiarity of the KKW-3 model: when WSP occurs in this model, the vehicle speeds and the flow rates in this WSP are usually related to points in the flow–density plane which are in the vicinity or lie on the boundary L in the flow–density plane (figure 2(*a*)), which corresponds to the synchronization distance D (see circles in figure 16(*b*)). Presumably, this behaviour is not a common feature of WSP, but due to the simplicity of the model.

(v) As in the diagram in [24], at higher flow rate q_{on} and lower flow rate q_{in} between the boundaries $F_S^{(B)}$ and $S_J^{(B)}$ the LSP occurs. The downstream front of LSP is localized at the

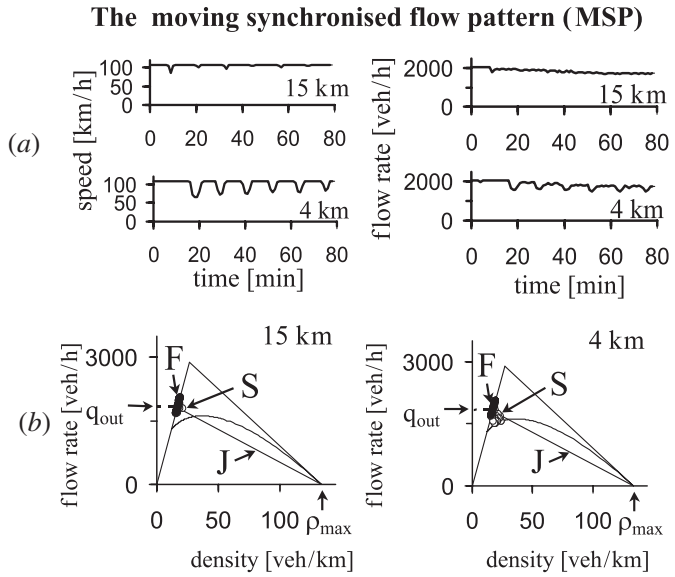

Figure 17. The moving synchronized flow pattern (MSP) related to figure 15(*d*) (KKW-3 model): (*a*) the vehicle speed (left) and the flow rate (right), (*b*) the corresponding data on the flow–density plane. One minute averaged data of virtual detectors, whose coordinates are indicated in (*a*, *b*).

on-ramp. However, the upstream front of LSP is not continuously moving upstream, so that the width of LSP remains spatially limited (figures 6 and 7(*f*)). Note that the upstream front of LSP and therefore the width of LSP can oscillate in time. Moreover, at flow rates close to the boundary $F_S^{(B)}$, fluctuations can cause random appearance and disappearance of LSP. The boundary which separates the region of WSP (see figures 6 and 11) from the region of LSP is marked by the letter *W* in the diagram of congested patterns.

4.4. General patterns (GP)

Right of the boundaries $S_J^{(B)}$ and *G* in figures 6 and 11 one finds the 'general pattern' (GP). It is a *self-maintaining* congested pattern, where synchronized flow occurs upstream of the on-ramp, and wide moving jams spontaneously emerge in this synchronized flow (figures 7(*a*) and (*b*), figure 8, figures 12(*a*) and (*b*) and figures 13 and 15(*a*)). In other words, in the GP wide moving jams are continuously generated somewhere upstream of the on-ramp. In the outflow of the wide moving jams either synchronized flow or free flow occurs. GP in the KKW models within the three-phase traffic theory have common features, which are very similar to those found in [24], as follows.

(i) If free flow occurs in the outflow of a wide moving jam, then the mean velocity of the downstream jam front v_g and the mean flow rate in the jam outflow q_{out} are characteristic quantities of the model. They do not depend on initial conditions and are the same for different wide moving jams. The mean velocity of the downstream front remains a characteristic parameter, no matter what the state of flow in the jam outflow is.

(ii) If $q_{in} > q_{out}$, then it is obvious that the width of the wide moving jam, which is furthest upstream, increases monotonously (figures 7(*a*), 8(*b*) and 12(*a*)). If in contrast $q_{in} < q_{out}$, the width of the most upstream wide moving jam decreases and this jam dissolves. This process of wide moving jam dissolution repeats for the next most upstream jam and so on (figures 7(*b*) and 12(*b*)). Nevertheless, if the difference between q_{out} and q_{in} is not very large, the region of

wide moving jams is widening upstream over time (figures 7(*b*) and 12(*b*)). Thus, GP which is very similar to the GP found in [24] spontaneously occurs in all CA models (table 1) within three-phase traffic flow theory under consideration. However, there are some peculiarities of the KKW models which will be considered below.

(iii) The first peculiarity of the KKW models considered here is linked to the fact mentioned above that the upstream front in WSP which separates synchronized flow downstream and free flow upstream moves with a very high (non-realistic) negative velocity. Let us consider a case, in which the flow rate q_{in} is high (it corresponds to a point above the boundary W, figures 6 and 11) and the flow rate q_{on} is related to a point right of the boundary $S_J^{(B)}$ in the diagram of congested patterns. In this case, first WSP occurs which further transforms into the GP, i.e. wide moving jams spontaneously emerge inside the synchronized flow of the initial WSP (figures 7(*a*) and 12(*a*)). However, the upstream front of this initial WSP moves considerably faster upstream than the fronts of any wide moving jam. For this reason, the upstream front of the whole GP at any flow rate q_{in} is determined by this upstream front of synchronized flow rather than by the most upstream wide moving jam. In figure 8 this upstream front of the synchronized flow is marked by the dashed line. Note that such a GP has been observed in empirical observations (see figure 20 and section V.A in [8]). In all CA models within the three-phase traffic theory under consideration, GP possesses similar non-linear features (compare figures 7(*a*) and (*b*) with figures 12(*a*) and (*b*) and figure 15(*a*), and figure 8 with figure 13).

(iv) There is also some difference in the GP formation in the continuous model [24] and in the KKW models in the three-phase traffic theory. This difference concerns the boundary G which separates the dissolving general pattern (DGP) and the GP.

Recall that DGP appears right of the boundary $S_J^{(B)}$ at the initial flow rate $q_{\text{in}} > q_{\text{out}}$. In this case, after a wide moving jam has been formed in synchronized flow upstream of the on-ramp, the mean flow rate in the jam outflow cannot exceed q_{out}. Thus, the initial condition $q_{\text{in}} > q_{\text{out}}$ is not fulfilled any more. As a result, the GP transforms into DGP, where one or several wide moving jams propagate upstream, and either free flow or one of SP occurs upstream of the on-ramp. This behaviour is realized also in the KKW models (figures 7(*c*) and 12(*c*)).

In [24] the boundary G intersects the boundary $S_J^{(B)}$ in the point $q_{\text{in}} = q_{\text{out}}$. In the CA models under consideration, however, the boundary G is shifted to the left in the diagram of congested patterns, i.e. the boundary G intersects the boundary $S_J^{(B)}$ at some $q_{\text{in}} > q_{\text{out}}$ (figures 6 and 11).

This behaviour may be explained by hysteresis effects or by the influence of high amplitude fluctuations (see the related remark at the end of section VII.B.1 in [8]). Indeed, in comparison with the model in [24] in the CA models, model fluctuations are very high. High amplitude fluctuations occur also in the outflow of a wide moving jam. This may explain why for $q_{\text{in}} > q_{\text{out}}$ right of the boundary $S_J^{(B)}$ still the general pattern rather than DGP may occur at considerably lower flow rate to the on-ramp q_{on} than in the model in [24].

(v) In some cases the GP, like that shown in figure 7(*b*), i.e. the GP where the most upstream jam is dissolved in the course of time, can occur even if the initial flow rate q_{in} is slightly higher than q_{out}. This is linked to the fact mentioned in item (iii) above that the upstream front of synchronized flow in the GP propagates upstream faster than that of any wide moving jam (see figures 7(*a*) and (*b*) and figure 8(*b*), where this upstream front is marked by the dashed line). Thus, upstream of the most upstream wide moving jam in GP a synchronized flow is formed. The flow rate in this synchronized flow, $q_{\text{in}}^{(\text{syn})}$, is always lower than the initial flow rate q_{in}. The latter flow rate is realized upstream of the upstream front of synchronized flow in GP (figures 7(*a*) and (*b*)). Therefore, the flow rate downstream of

the upstream front of synchronized flow in GP, i.e. the flow rate $q_{\rm in}^{(\rm syn)}$, is the incoming flow rate for the most upstream wide moving jam rather than the initial flow rate $q_{\rm in}$. It can occur that $q_{\rm in}^{(\rm syn)}$ is also lower than $q_{\rm out}$. In this case, the most upstream wide moving jam in GP will be dissolved.

For the KKW-1 model (parameter-set I of table 3) the maximal value of the flow rate $q_{\rm in}$ at which GP of this type occurs is 1960 vehicles/h. For the KKW-2 model this flow rate $q_{\rm in}$ is very close to the flow rate $q_{\rm out} = 1810$ vehicles/h. For the KKW-3 model this flow rate is $q_{\rm in} = 2160$ vehicles/h.

(vi) In empirical observations of GP at on-ramps, it has recently been found [8] that GP possesses the following characteristic feature: if the flow rate to the on-ramp $q_{\rm on}$ is high enough, the average flow rate in the pinch region $q^{(\rm pinch)}$ (averaged over a time interval which is considerably larger than the time distance between narrow moving jams emerging in the pinch region of GP) reaches the limit flow rate $q_{\rm lim}^{(\rm pinch)}$. This means that the flow $q^{(\rm pinch)}$ does not decrease below $q_{\rm lim}^{(\rm pinch)}$ even if the flow rate $q_{\rm on}$ further increases. This case is called the 'strong' congestion [8]. In the strong congestion condition, GP cannot exist if $q_{\rm in} < q_{\rm lim}^{(\rm pinch)}$ [8, 45]. Note that in the 'weak' congestion condition which is realized at lower flow rates $q_{\rm on}$ the flow rate $q^{(\rm pinch)}$ changes noticeably when the flow rate $q_{\rm on}$ is changing.

As in the model [24], both the strong congestion and the weak one can be simulated in the KKW models under consideration. In particular, GP cannot exist if $q_{\rm in} < q_{\rm lim}^{(\rm pinch)}$. Indeed, at high flow rates to the on-ramp $q_{\rm on}$ the boundary $S_J^{(B)}$ transforms into a horizontal line at $q_{\rm in} = q_{\rm lim}^{(\rm pinch)}$ (figures 6 and 11). For the KKW-1 model (parameter-set I of table 3) we obtain $q_{\rm out}/q_{\rm lim}^{(\rm pinch)} \approx 1.57$. This value is also approximately in accordance with the empirical finding (see the empirical formula (4) in [8]).

It should be noted that in the vicinity of this horizontal line on the boundary $S_J^{(B)}$, after the GP has been formed (precisely, when the related point in the flow–flow plane in figures 6 and 11 has been moved above and right of the boundary $S_J^{(B)}$), the strong congestion in the pinch region occurs, and the flow rate of the vehicles, which may actually squeeze to the road from the on-ramp, can decrease in comparison with the initial flow rate $q_{\rm on}$. This effect has also occurred in the model [24] at the related high initial flow rates $q_{\rm on}$. Nevertheless, the GP remains the GP after this decrease in the real $q_{\rm on}$. This is due to a hysteresis effect in the flow rate to the on-ramp $q_{\rm on}$ which accompanies the occurrence and the disappearance of the GP when the flow rate $q_{\rm on}$ first increases and then decreases, correspondingly. However, the detailed investigation of hysteresis effects is out of the scope of this paper and it will be considered elsewhere.

4.5. Probability of the breakdown phenomenon (the F → S transition) at the on-ramp

Let us first recall how the breakdown phenomenon looks like in the fundamental diagram approach. From a numerical analysis of a macroscopic traffic flow model within the fundamental diagram approach, Kerner and Konhäuser found in 1994 [33] that free flow is metastable with respect to the formation of wide moving jams (F → J transition), if the flow rate is equal to or higher than the outflow from a jam, $q_{\rm out}$. The critical amplitude of a local perturbation in an initially homogeneous free flow, which is needed for the F → J transition, decreases with increasing density; it is maximal at the threshold density $\rho = \rho_{\rm min}$, below which free flow is stable. $\rho_{\rm min}$ is the characteristic density in the outflow from a wide moving jam, i.e. when $q = q_{\rm out}$. The critical amplitude becomes zero at some critical density $\rho = \rho_{\rm cr} > \rho_{\rm min}$, above which free flow is linearly unstable. Obviously, the higher the amplitude of a random local perturbation the less frequent it is. Hence, the likelihood that the F → J transition occurs

in a given time interval should increase with density (or flow rate). The probability should be very small at the threshold density $\rho_{\min}$ (at the threshold flow rate q_{out}), and it should tend to 1 at the critical density ρ_{cr} (at the related critical flow rate in free flow).

In 1997 Mahnke *et al* [53, 54] developed a master equation approach for calculating the probability of the F $\rightarrow$ J transition on a homogeneous road (i.e. without bottleneck). Based on this approach, Kühne *et al* [55] confirmed that the probability of the F $\rightarrow$ J transition in the metastable region is increasing with the flow rate in free flow. They applied this result to explain the breakdown phenomenon at a highway bottleneck. For a recent comprehensive discussion of the breakdown phenomenon in CA models and in the Krauß *et al* model in the fundamental diagram approach, see also [56, 57]. The theories in [33, 53–57] belong to the fundamental diagram approach.

In contrast to these results, in Kerner's three-phase traffic theory [3, 42, 43] it is postulated that metastable states of free flow decay into synchronized flow (F $\rightarrow$ S transition) rather than wide moving jams (F $\rightarrow$ J transition). Moving jams can emerge spontaneously only in synchronized flow, i.e. after a sequence of F $\rightarrow$ S$\rightarrow$ J transitions [6]. In particular, even the upper limit of free flow, $q_{\max}$, is related to the F $\rightarrow$ S transition: in this limit point, the probability of the F $\rightarrow$ S transition should be approximately equal to 1 whereas the probability of the emergence of a moving jam (F $\rightarrow$ J transition) should be very small. Thus, in this theory the breakdown phenomenon in free traffic is related to the F $\rightarrow$ S transition rather than to an emergence of moving jams.

In the three-phase traffic theory, it is also postulated that the breakdown phenomenon at a highway bottleneck (i.e. due to an on-ramp) is due to a localized deterministic perturbation at the bottleneck [7]. Indeed, due to this perturbation the probability of the F $\rightarrow$ S transition should be considerably higher at the bottleneck than anywhere else. Thus, in this theory there is a spatially non-homogeneous distribution of the probability of the breakdown phenomenon (of the F $\rightarrow$ S transition) on a road (per unit of space and time): at effective bottlenecks on the road, the probability of the breakdown phenomenon should have a maximum (see figure 1(*b*) in [7]). This explains why the breakdown phenomenon mostly occurs at highway bottlenecks.

In the following, we confirm these hypotheses of three-phase traffic theory for the KKW models proposed in this paper. In particular, we find that a localized permanent perturbation indeed occurs in the vicinity of the bottleneck (due to the on-ramp), and that it triggers the breakdown of initial free flow at the on-ramp rather than anywhere else.

As in [24], at the boundary $F_S^{(B)}$ the F $\rightarrow$ S transition occurs at the on-ramp. Due to this transition the vehicle speed decreases sharply at the on-ramp. A sharp drop in vehicle speeds at the on-ramp (or at another bottleneck) is well known from empirical observations (e.g. [58, 59]). Traffic engineers have called this effect 'the breakdown phenomenon' in traffic flow. The F $\rightarrow$ S transition has the nature of such a breakdown phenomenon.

In [24] it was also shown that the F $\rightarrow$ S transition resembles a first order phase transition: it requires nucleation, i.e. the occurrence of a local perturbation in traffic flow whose amplitude exceeds some critical value. This critical amplitude is a decreasing function of the vehicle density in free flow (see the curve F_S in figure 1(*b*) in [24]). The higher the amplitude of a random perturbation (fluctuation) the less likely it is, with a probability distribution that for very general reasons can be assumed to decay exponentially for large amplitudes. Therefore we expect that the probability that the F $\rightarrow$ S transition happens within a given time interval increases exponentially with the vehicle density in free flow.

Such behaviour of the probability of the breakdown phenomenon, i.e. the F $\rightarrow$ S transition, has indeed been observed empirically by Persaud *et al* [59]. In the case of the on-ramp, however, there is already a local permanent non-homogeneity, which occurs due to the squeezing of vehicles into the main road. Corresponding to [7] this should explain why

the F $\rightarrow$ S transition occurs at the on-ramp with a considerable higher probability than away from the on-ramp at the same flow rate.

This local permanent (deterministic) perturbation at on-ramp determines the character of the boundary $F_S^{(B)}$ [8]. The higher the flow rate to the on-ramp $q_{\rm on}$, the higher is the amplitude of this permanent perturbation. Therefore, the higher the flow rate to the on-ramp $q_{\rm on}$, the lower is the flow rate $q_{\rm in}$ on the main road upstream of the on-ramp, at which the related critical amplitude occurs at the bottleneck; this may explain the negative slope of the curve $F_S^{(B)}$ in the flow–flow plane in figure 6(a).

However, a real local perturbation which leads to the F $\rightarrow$ S transition at the on-ramp has always also a random component, i.e. the real local perturbation should consist of two components: (a) a permanent perturbation, the amplitude of which is higher, the higher the flow rate to the on-ramp $q_{\rm on}$ is, and (b) a random component. The latter component should lead to the F $\rightarrow$ S transition at the on-ramp with some probability also, if the flow rate upstream of the on-ramp, $q_{\rm in}$, and the flow rate to the on-ramp, $q_{\rm on}$, belong to points in the flow–flow plane in figure 6(a) which lie to the *left* of the boundary $F_S^{(B)}$, i.e. still in the free flow region. This probability should increase, if the flow rate $q_{\rm sum} = q_{\rm in} + q_{\rm on}$ approaches the boundary $F_S^{(B)}$. At the boundary $F_S^{(B)}$ the probability is approximately equal to 1. If these assumptions are correct, then the probability of the F $\rightarrow$ S transition at the on-ramp must grow, if the flow rate upstream of the on-ramp $q_{\rm in}$ increases at a given constant flow rate to the on-ramp $q_{\rm on}$, which can be related to the results of empirical observations [59].

To study the probability of the F $\rightarrow$ S transition at the on-ramp (figure 18) in the KKW-1 model (parameter-set I of table 3) a large number of runs of the same duration T_0 have been studied for given flow rates $q_{\rm sum}$ and $q_{\rm on}$. At the beginning of each run, there was free flow at the on-ramp. For each run it was checked, whether the F $\rightarrow$ S transition at the on-ramp occurred within the given time interval T_0 or not. The result of these simulations is the number of realizations $n_{\rm P}$ where the F $\rightarrow$ S transition at the on-ramp had occurred in comparison with the number of all realizations $N_{\rm P}$. Then

$$P_{\rm FS} \approx n_{\rm P}/N_{\rm P} \tag{25}$$

is the approximate probability that the F $\rightarrow$ S transition at the on-ramp in an initial free flow occurs during the time interval T_0 at given flow rates $q_{\rm sum}$ and $q_{\rm on}$. Equation (25) converges towards the probability for $N_{\rm P} \rightarrow \infty$.

The flow rate $q_{\rm sum}$ was changed and the procedure with all realizations was repeated at the same flow rate to the on-ramp $q_{\rm on}$. The flow rate $q_{\rm sum}$ at which the F $\rightarrow$ S transition at the on-ramp occurred in all realizations is therefore related to $P_{\rm FS} \approx 1$. The probability $P_{\rm FS} \approx 1$ for $T_0 = 30$ min corresponds to a point on the boundary $F_S^{(B)}$ in the diagram of congested patterns in figure 6(a).

We found that lower flow rates $q_{\rm sum}$ correspond to $P_{\rm FS} < 1$. As expected above, we found indeed an exponential increase of $P_{\rm FS}$ as a function of the flow rate $q_{\rm sum}$ at a given flow rate to the on-ramp $q_{\rm on}$. This confirms the above assumptions [7] about the nature of the breakdown phenomenon at the on-ramp. However, for $P_{\rm FS}$ close to 1 there are deviations from the exponential increase, which will be discussed elsewhere.

Figure 18 shows that the nucleation rate is higher, the larger the $q_{\rm on}$ is. This can be inferred from the fact that the range of flow rates downstream, $q_{\rm sum}$, over which the nucleation probability changes by a given amount, is much narrower for higher $q_{\rm on}$. The stronger permanent perturbation (higher $q_{\rm on}$) acts like a bias which makes it easier to overcome the nucleation barrier.

The F $\rightarrow$ S transition leads to the occurrence of different synchronized flow patterns upstream of the on-ramp which have been considered above.

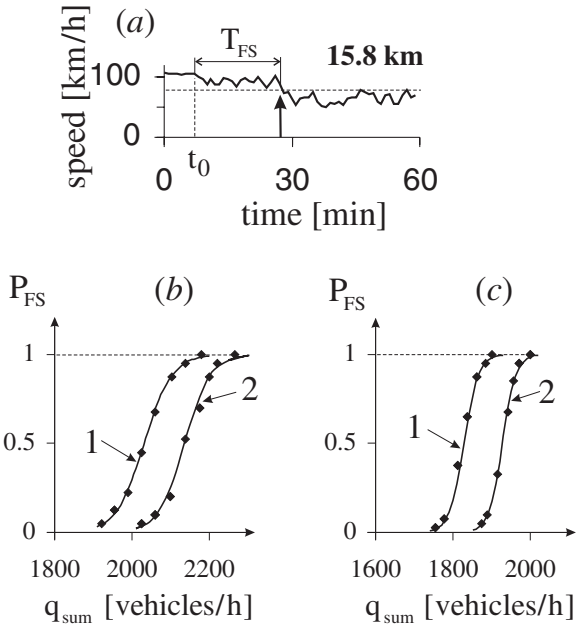

Figure 18. Probability of breakdown phenomenon at the on-ramp for the KKW-1 model (parameter-set I of table 3): (*a*) time dependence of the vehicle speed, when the F → S transition occurs at the on-ramp (the arrow marks the F → S transition). Data are one minute averages of a virtual detector located at $x = 15.8$ km (200 m upstream of the start of the on-ramp merging area). The dashed line shows the speed level 80 km h^{-1}; the characteristic duration of a sharp decrease in the vehicle speed (this 'breakdown' is marked by the arrow) is about 1–2 min in agreement with empirical observations. (q_{on}, q_{in}) have the following values: (200, 1660) vehicles/h. (*b*, *c*) The probability P_{FS} that the F → S transition occurs at the on-ramp within $T_0 = 30$ min (curve 1) or already within $T_0 = 15$ min (curve 2), after the on-ramp inflow was switched on (at $t_0 = 8$ min), versus the traffic demand upstream of the on-ramp, $q_{sum} = q_{min} + q_{on}$. Results are shown for two different flow rates to the on-ramp, $q_{on} = 60$ vehicles/h in (*b*) and $q_{on} = 200$ vehicles/h in (*c*). The following criterion that a F → S transition has occurred is used: The vehicle speed just upstream of the on-ramp drops below the level 80 km h^{-1} and then remains at nearly the same low level for more than 4 min (cf (*a*)). The probabilities were obtained from $N_P = 40$ independent runs. The curves in (*b*, *c*) are fits with the function $(1 + \tanh(\alpha(q_{sum} - q_P)))/2$. The values ($\alpha$, q_P) are: (*b*) curve 1 (0.014, 2031) and curve 2 (0.015, 2135), (*c*) curve 1 (0.027, 1828) and curve 2 (0.029, 1927).

4.6. The capacity drop

Empirical observations show that the speed breakdown at a bottleneck is in general accompanied by a drop in highway capacity. If there is free rather than congested flow upstream of the bottleneck, the highway capacity is usually higher. This phenomenon is called 'the capacity drop' (for a review see [58]).

As explained in the previous section, the breakdown phenomenon in three-phase traffic theory is a F → S transition at the bottleneck, so that the capacity drop is the difference between highway capacity in free flow and in a situation, where there is synchronized flow upstream and free flow downstream of the bottleneck [7, 42]. Thus the capacity drop is *not* determined by the outflow q_{out} from a wide moving jam in contrast to the fundamental diagram approach.

Obviously, in order to study the capacity drop one has to consider the outflow from a congested bottleneck $q_{out}^{(bottle)}$, which is measured downstream of the bottleneck, where free flow conditions are reached. In this paper, we consider the special example of an on-ramp

as bottleneck. In [7] Kerner points out that $q_{\rm out}^{\rm (bottle)}$ is not just a characteristic property of the type of bottleneck under consideration. It also depends on the type of congested pattern which actually is formed upstream of the bottleneck (as well as on the features of the congested pattern). The type of congested pattern and the pattern features depend on the flow rates $q_{\rm on}$ and $q_{\rm in}$. Hence, in the case of an on-ramp, $q_{\rm out}^{\rm (bottle)}$ is expected to vary with $(q_{\rm on}, q_{\rm in})$. Obviously, $q_{\rm out}^{\rm (bottle)}$ only limits the highway capacity (this highway capacity can be called 'congested pattern capacity'), if it is smaller than the traffic demand upstream of the on-ramp, $q_{\rm sum} = q_{\rm in} + q_{\rm on}$, i.e. if the condition

$$q_{\rm out}^{\rm (bottle)}(q_{\rm on}, q_{\rm in}) < q_{\rm sum}(q_{\rm on}, q_{\rm in}) \tag{26}$$

is fulfilled. Then the congested pattern upstream from the on-ramp simply expands, while the throughput remains limited by $q_{\rm out}^{\rm (bottle)}$. For example, if the general pattern (GP) is formed at the bottleneck, an increase of $q_{\rm in}$ does not influence the discharge flow rate $q_{\rm out}^{\rm (bottle)}$. Instead, the width of the wide moving jam, which is most upstream in the general pattern, simply grows.

Assuming that (26) is fulfilled, the capacity drop is given by

$$\Delta q = q_{\rm max} - q_{\rm out}^{\rm (bottle)} \tag{27}$$

where $q_{\rm max}$ denotes the highway capacity in free flow, i.e. the maximum flow rate in free flow. The minimum value, which $q_{\rm out}^{\rm (bottle)}$ can take, if one considers all kinds of congested patterns upstream from a bottleneck, should be a characteristic quantity for the type of bottleneck under consideration. We denote this quantity by $q_{\rm min}^{\rm (bottle)}$. The maximum of $q_{\rm out}^{\rm (bottle)}$ (denoted by $q_{\rm max}^{\rm (bottle)}$) is predicted to be the maximum flow rate, which can be realized in synchronized flow [7], $q_{\rm max}^{\rm (bottle)} = q_{\rm max}^{\rm (syn)}$. Hence, the capacity drop at a bottleneck cannot be smaller than

$$\Delta q_{\rm min} = q_{\rm max} - q_{\rm max}^{\rm (syn)}. \tag{28}$$

This general picture of the capacity drop proposed by Kerner for the three-phase traffic theory [7, 52] has been confirmed by empirical investigations [7, 8] and in numerical studies of congested patterns at an on-ramp [24], as well as in this paper.

In particular, we found that for the KKW-1 model (parameter-set I of table 3) $q_{\rm max}^{\rm (syn)} \approx$ 2250 vehicles/h. This flow rate corresponds to WSP at $q_{\rm in} = q_{\rm max}$ and low flow rate to the on-ramp ($q_{\rm on} \approx 10$ vehicles/h). The flow rate $q_{\rm min}^{\rm (bottle)} \approx 1600$ vehicles/h is related to LSP. Thus, the discharge flow rate $q_{\rm out}^{\rm (bottle)}$ in (27) can be changed in the range from 1600 to 2250 vehicles/h. As the capacity of the highway in free flow (for parameter-set I) is $q_{\rm max} \approx 2400$ vehicles/h, the capacity drop (27) can vary in the range from 150 to 800 vehicles/h, depending on the type of congested pattern and the pattern parameters. In comparison with free flow conditions, the capacity drops by 6.25% for WSP at low flow rate to the on-ramp up to 33.3% for LSP at a high flow rate to the on-ramp.

To show the dependence of the capacity drop on the congested pattern type and the pattern parameters more clearly, let us consider a specific example: initially the flow to the on-ramp, $q_{\rm on} = 60$ vehicles/h, is low, and the flow rate upstream of the on-ramp, $q_{\rm in} = 2160$ vehicles/h, is relatively high. As a result, WSP occurs (figure 6(*a*)). In this case, the discharge flow rate $q_{\rm out}^{\rm (bottle)} = 1950$ vehicles/h, i.e. the capacity drop (27) is $\Delta q = 210$ vehicles/h. Let us now increase traffic demand upstream of the on-ramp, i.e. the flow rate $q_{\rm on}$ increases up to $q_{\rm on} = 120$ vehicles/h but the flow rate $q_{\rm in} = 2160$ vehicles/h remains the same. This causes the flow rate of synchronized flow in WSP to decrease *more* than the traffic demand $(q_{\rm in} + q_{\rm on})$ increases. For this reason, although the flow rate $q_{\rm on}$ increases, the discharge flow rate *decreases*: $q_{\rm out}^{\rm (bottle)} = 1800$ vehicles/h. This leads to a larger capacity drop (27): $\Delta q = 360$ vehicles/h.

If now the flow rate q_{on} is further increased up to $q_{\mathrm{on}} = 240$ vehicles/h (the flow rate $q_{\mathrm{in}} = 2160$ vehicles/h remaining unchanged), WSP transforms into GP (figure 6(*a*)). This leads to a further decrease in the discharge flow rate, $q_{\mathrm{out}}^{(\mathrm{bottle})} = 1700$ vehicles/h, which is due to the pinch effect in synchronized flow of GP. The pinch effect strongly reduces the flow rate through the pinch region of the GP. The capacity drop (27) increases to $\Delta q = 460$ vehicles/h.

If the flow rate q_{on} is once more increased up to $q_{\mathrm{on}} = 900$ vehicles/h and the flow rate q_{in} remains the same, strong congestion occurs in the pinch region of the GP. This decreases the discharge flow rate to $q_{\mathrm{out}}^{(\mathrm{bottle})} = 1630$ vehicles/h. Thus the capacity drop (27) increases to $\Delta q = 530$ vehicles/h. In all cases considered here condition (26) is fulfilled.

It must be noted that there may be one exception to condition (26) [52]. If LSP (the localized synchronized flow pattern) occurs both on the main road and on the on-ramp upstream of the merge region of the on-ramp then the discharge flow rate is equal to traffic demand:

$$q_{\mathrm{out}}^{(\mathrm{bottle})}(q_{\mathrm{on}}, q_{\mathrm{in}}) = q_{\mathrm{sum}}(q_{\mathrm{on}}, q_{\mathrm{in}}). \tag{29}$$

The congested pattern capacity which is related to this LSP should be determined by the maximal discharge flow rate at which the LSP still exists upstream of the on-ramp.

5. Discussion

The numerical simulations of the CA models within the three-phase traffic theory, which we have developed in this paper, show that the basic vehicle motion rules (1), (3) introduced by Kerner and Klenov in [24] for a microscopic three-phase traffic theory allow a *variety of simple specifications* for the synchronization distance, the fluctuations and for the vehicle acceleration and deceleration which lead to *qualitatively the same diagram of congested patterns and to the same pattern features* at on-ramps. This is due to the introduction of the synchronization distance D in the basic vehicle motion rules (1), (3), which leads to a 2D region of steady states in the flow density plane. The robustness of the phenomena with respect to different specifications of the model details leads to the expectation that these phenomena occur generically independent of, e.g., the different laws and driver behaviours in different countries.

In the KKW model formulation of three-phase traffic theory based on these basic vehicle motion rules (1), (3) specific functions for fluctuations and for the vehicle acceleration and deceleration can be very simple. Nevertheless, the main features of the diagrams of congested patterns, which these CA models show, are qualitatively the same as recently found within the three-phase traffic theory and in empirical observations [8, 45].

In [24] it has been shown that these pattern features and the related diagram of congested patterns at on-ramps in the three-phase traffic theory are qualitatively different in comparison with the diagram by Helbing *et al* [1, 10], which has been derived for a wide class of traffic flow models within the fundamental diagram approach. In particular, in that diagram of congested patterns (congested states) near a boundary which separates trigger stop-and-go traffic (TSG) and oscillating congested traffic (OCT) (in the terminology of [1, 10]) a congested pattern which is a 'mixture' of TSG, OCT and HCT (homogeneous congested traffic) should occur [1]. This pattern, which at first sight looks like GP, has been used in [1] for an explanation of the pinch effect in synchronized flow and for the jam emergence observed in [6]. However, this mixture pattern has no own region in the diagram of states in [1, 10, 15]: the pattern transforms into TSG, if q_{on} decreases, or into OCT or else HCT, if q_{on} increases. In our diagrams (figures 6 and 11 and in [24, 8]) there are no TSG, no OCT and no HCT. Instead, GP exists in a very large range of flow rates q_{on} and q_{in}. At a given q_{in} GP in the three-phase traffic theory does not transform into another congested

pattern, even if q_{on} increases up to the highest possible values. Thus GP in the CA models under consideration and in [8, 24] has a qualitatively different nature in comparison with the mixture of TSG, OCT and HCT in [1, 10]. Note that empirical observations of congested patterns at on-ramps [8] confirm the theoretical features of GP found within the three-phase traffic theory [8, 24], rather than the theoretical features of either TSG, OST or HCT, or else of the mixture of TSG, OST and HCT within the fundamental diagram approach derived in [1, 10, 15].

In 2000, Knospe *et al* [22] proposed a version of the NaSch model where in addition to the previous versions (e.g. [39]) drivers react at intermediate distances to speed changes of the next vehicle downstream, i.e. to 'brake lights'. The steady states of this model with 'comfortable driving' belong to a fundamental diagram, i.e. the NaSch model with 'comfortable driving' is a CA model in the fundamental diagram approach. The NaSch model with 'comfortable driving' has been applied in [22, 23, 47] for a description of three traffic phases: free flow, synchronized flow and wide moving jams.

In order to compare this model with those investigated here, the congested patterns, which spontaneously occur at an on-ramp, and their evolution, when the flow rate to the on-ramp is changing, were calculated for the NaSch CA model with 'comfortable driving' [22, 23, 47]. These new results will be discussed below. It will be shown that both the diagrams of congested patterns and the pattern features of the KKW models in three-phase traffic theory are qualitatively different from those obtained for the NaSch CA model with 'comfortable driving', with one exception, concerning the wide moving jam propagation, which will be discussed first.

5.1. Wide moving jam propagation

The characteristic parameters of wide moving jam propagation which were found in empirical observations [4, 7, 41, 60] can be reproduced in many traffic flow models in the fundamental diagram approach, where they have first been predicted by Kerner and Konhäuser in 1994 [33] (see also the later papers by Bando, Sugiyama *et al* [61], by Krauß *et al* [46], by Barlovic *et al* [39], and the reviews by Chowdhury *et al* [2] and by Helbing [1]). As already mentioned, the slow-to-start rules [22, 39, 51] allow the wide moving jam propagation through different traffic states and bottlenecks keeping the characteristic velocity of the downstream jam front. This effect has recently been simulated in the NaSch model with 'comfortable driving' [23]. This is in accordance with empirical observations and the wide moving jam definition made above [4, 7, 41]. Because the slow-to-start rules [22, 39] are used in our CA models as well, these CA models within the three-phase traffic theory also show the effect of the wide moving jam propagation through different congested patterns and bottlenecks (figure 19). In particular, if a wide moving jam which has been formed upstream of the on-ramp (the jam is marked as 'foreign' wide moving jam in figure 19) then the jam propagates through the on-ramp and through GP (figure 19(*a*)) and also through WSP (figure 19(*b*)) keeping the velocity of the downstream front of the jam.

However, the effect of the wide moving jam propagation [41] as well as the other characteristic parameters of wide moving jams are apparently the *only features* which are the same in the fundamental diagram approach [23, 33, 39, 46] and in the three-phase traffic theory [4, 62]. All other known features of congested patterns which spontaneously occur upstream of the on-ramp and their evolution for the NaSch CA model with 'comfortable driving' [22, 23, 47] are qualitatively different from those, which follow from the KKW models within the three-phase traffic theory, as will be shown in the next section. This is due to the principal difference between the non-linear features of congested traffic in the NaSch

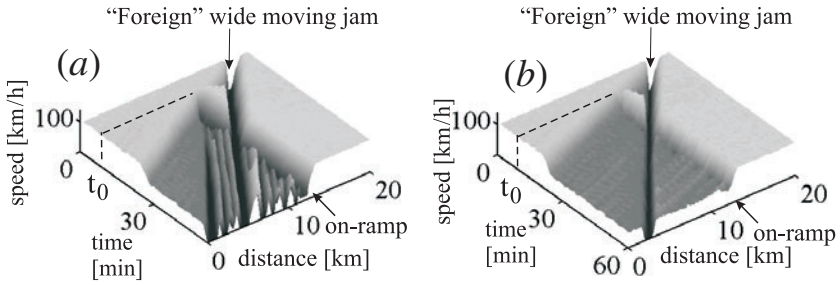

Figure 19. Simulation of the propagation of a 'foreign' wide moving jam: (*a*) propagation through GP, (*b*) propagation through WSP. The on-ramp is located at $x = 12$ km, and the inflow is switched on at $t_0 = 7$ min. The flow rates (q_{on}, q_{in}) are: (*a*) (480, 2300) and (*b*) (110, 2160). The initial location of the 'foreign' wide moving jam is $x = 18$ km, the initial jam length is 0.7 km. Single vehicle data are averaged over a space interval of 40 m and a time interval of 1 min. KKW-1 model (table 1): parameter k of the synchronization distance D_n is $k = 2.55$ for (*a*) and $k = 4$ for (*b*). Other model parameters are given in table 3, parameter-set I.

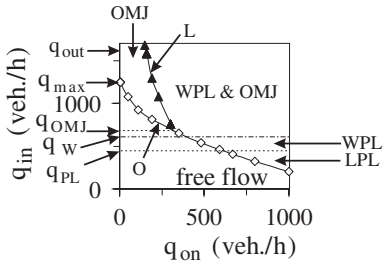

Figure 20. Diagram of congested patterns at the on-ramp for the NaSch CA model with comfortable driving. OMJ—oscillating moving jams, WPL—widening pinned layer, LPL—localized pinned layer. The parameters of the model are taken from [22, 23]: in particular, the maximal speed $v_{free} = 27$ m s^{-1} ($v_{free} = 97.2$ km h^{-1}), the minimal distance $d = 7.5$ m, the time step $\tau = 1$ s, the maximum flow rate $q_0 = 2817$ vehicles/h and the flow rate out from the jam $q_{out} = 1580$ vehicles/h. The other specific parameters of the CA model with comfortable driving (notations as in [22, 23]) are $p_d = 0.1$, $p_b = 0.95$, $p_0 = 0.5$, $h = 8$, $\text{gap}_{security} = 3$, the cell length is 1.5 m. For the simulation of the on-ramp in the CA model with comfortable driving, the distance $dx_{on}^{(min)}$ is chosen as $dx_{on}^{(min)} = 4d$. The length of the road is 75 km, the on-ramp is at $x = 65.4$ km, the length of merging area is 0.6 km. As in figures 6 and 11, after the on-ramp has been switched on, there is a delay time for the congested pattern formation upstream of the on-ramp. However, here the boundaries O ('oscillating') and L ('layer') depend more strongly on the delay time which is chosen for awaiting the congested pattern to occur upstream of the on-ramp, after the on-ramp has been switched on. The boundary O is determined as the points (q_{on}, q_{in}), where either OMJ or WPL or LPL occurred upstream of the on-ramp in an initial flow with maximum speed $v = v_{free}$ within 20 min after the on-ramp has been switched on. The time interval for the determination of the boundary L was 60 min.The qualitative features of the diagram do not depend on these time intervals. The maximum flow rate in free flow $q_{max} = 1250$ vehicles/h.

model with 'comfortable driving' [22, 23] and in the KKW models within the three-phase traffic theory presented in our paper.

5.2. Comparison with congested patterns in the Nagel–Schreckenberg cellular automata models with 'comfortable driving'

In figures 20–24 we compare the congested patterns and their evolution obtained in the KKW models of three-phase traffic theory with those for a NaSch-type CA model with 'comfortable driving' with one lane, for which we use the rules and parameters presented in [22, 23, 47].

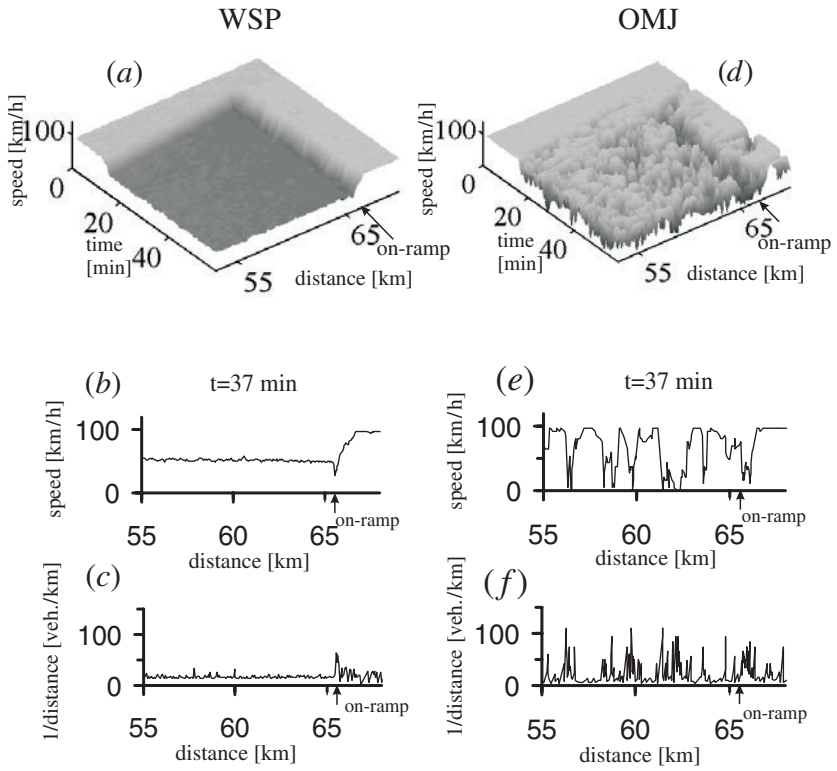

Figure 21. Comparison of the widening synchronized flow pattern (WSP) in our CA model within the three-phase traffic theory (*a–c*) with the oscillating moving jam pattern (OMJ) at the on-ramp in the NaSch CA model with comfortable driving (*d–f*). (*a*, *d*) The vehicle speed as function of distance and time; at $t_0 = 8$ min the on-ramp inflow is switched on. (*b*, *e*) The vehicle speed as function of distance at a given time. (*c*, *f*) The inverse distance between vehicles as function of distance along the road. In (*a–f*) single vehicle data are used. For (*a–c*), the KKW-1 model (table 1) with the following parameters is used: $k = 4.5$, $p = 0.04$, $p_0 = 0.5$, $v_p = 14$ m s^{-1}, $p_{a1} = 0.5$ and $p_{a2} = 0.05$. The parameter of the merging condition (21) at the on-ramp is $\lambda = 0.4$. For (*d–f*) the CA model with comfortable driving given in [22, 23, 47] was used. In both models, $v_{\text{free}} = 27$ m s^{-1}, $d = 7.5$ m, $\tau = 1$ s, $q_0 = 2817$ vehicles/h, $q_{\text{out}} = 1580$ vehicles/h (table 2), the length of the road is 75 km, the on-ramp is at $x = 65.4$ km, the length of merging area is 0.6 km. The other specific parameters of the CA model with comfortable driving are the same as in figure 20. With these parameters, one obtains the results in (*a–c*) for $(q_{\text{in}}, q_{\text{on}}) = (1246, 600)$ vehicles/h, in (*d–f*) for $(q_{\text{in}}, q_{\text{on}}) = (1246, 190)$ vehicles/h.

All calculations for the NaSch CA model with comfortable driving are made for two different models of the on-ramp: (1) the lane changing rules described in [23, 47] are applied, or (2) the model of the on-ramp described in section 4.1 is used. In the latter case the distance between two consecutive vehicles on the main road, which permits a vehicle to enter from the on-ramp, is chosen as $dx_{\text{on}}^{(\min)} = 4d$. This corresponds to the condition applied in [23, 47] that 'an effective gap to the predecessor and a gap to the successor on the destination lane' is larger than or equal to the vehicle length d. It has been found that all features of the congested patterns and their evolution, when the flow rate to the on-ramp is increasing, remain qualitatively the same for both models of the on-ramp. Therefore, only one set of results for the model of the on-ramp described in section 4.1 is shown in figures 20–24. This comparison shows the following results.

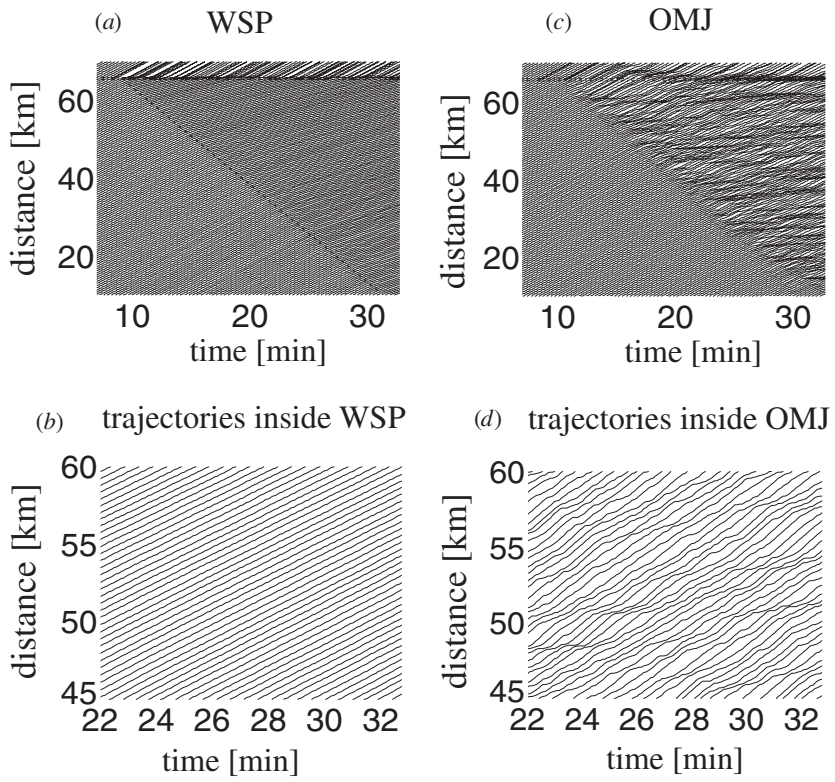

Figure 22. Comparison of the vehicle trajectories related to the patterns in figure 21: widening synchronized flow pattern (WSP) in the KKW-1 model (table 1) within the three-phase traffic theory (left), oscillating moving jams (OMJ) in the NaSch CA model with comfortable driving within the fundamental diagram approach (right). (*a*) Vehicle trajectories (overview) of WSP shown in figure 21(*a*). (*b*) Vehicle trajectories inside of WSP. (*c*) Vehicle trajectories (overview) of OMJ upstream of the on-ramp shown in figure 21(*d*). (*d*) Vehicle trajectories inside OMJ. Only trajectories of every 7th vehicle are shown.

(i) In the NaSch CA model with comfortable driving [23] without on-ramps and other bottlenecks, i.e. on a homogeneous one-lane road, when the flow rate is gradually increasing, the free flow motion spontaneously transforms into a very complex dynamical behaviour at some critical flow rate on the road, $q_{\max}$: if a narrow moving jam emerges spontaneously, this jam dissolves within a very short time interval (about one–two time steps, i.e. 1–2 s), then a new narrow moving jam emerges which again dissolves quickly and so on at different locations and at different times. This behaviour resembles the oscillating congested traffic which was reported for other traffic flow models within the fundamental diagram approach by Lee *et al* [11], Tomer *et al* [18] and in the diagram of congested patterns at on-ramps by Helbing *et al* [1, 10].

(ii) In the NaSch CA model with comfortable driving on a one-lane road with an on-ramp, a complex oscillation pattern occurs upstream of the on-ramp spontaneously for $q_{\text{in}} \geqslant q_{\max}$, which is qualitatively the same as in (i): narrow moving jams first emerge and then dissolve within a very short time interval at different highway locations and at different times. This pattern exists already for very small values of the flow rate to the on-ramp q_{on} (figure 20). We will call this pattern in the NaSch CA model with comfortable driving 'oscillating moving jams' (OMJ) (figures 21(*d*)–(*f*) and figures 22(*c*) and (*d*)).

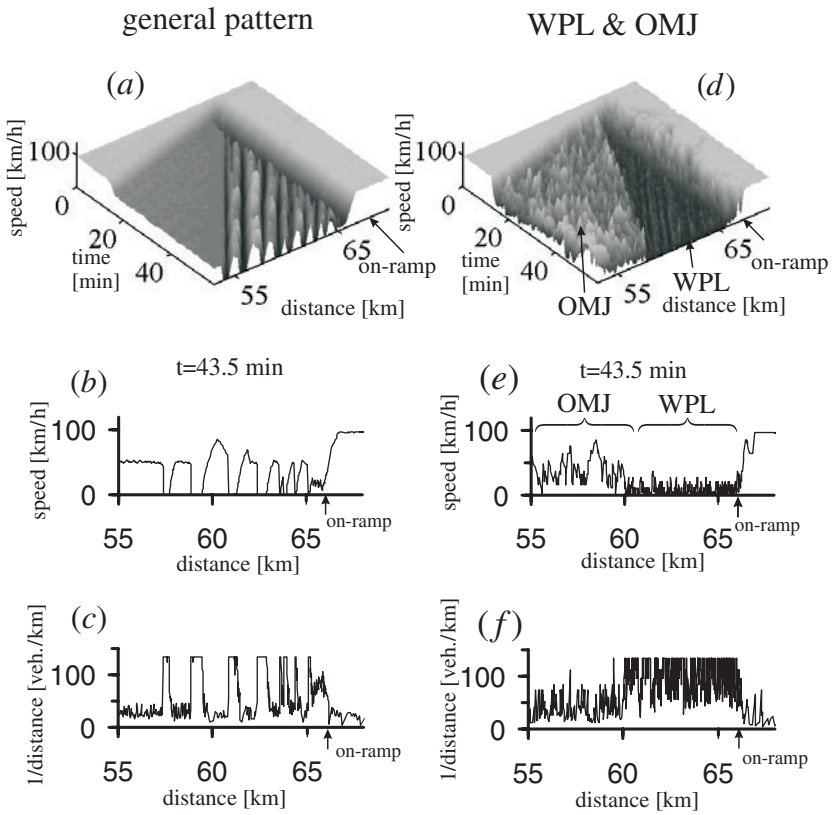

Figure 23. Comparison of the general pattern (GP) in the KKW-1 model (table 1) within the three-phase traffic theory (left) with the congested pattern at the on-ramp in the NaSch CA model with comfortable driving within the fundamental diagram approach (right). The latter consists of a widening pinned layer (WPL) going over into OMJ further upstream. (*a*, *d*) Vehicle speed as function of distance and time; at $t_0 = 1$ min the on-ramp inflow is switched on. (*b*, *e*) Vehicle speed as function of distance at a given time. (*c*, *f*) Inverse distance between vehicles as function of distance along the road. In (*a*–*f*) single vehicle data are used. The simulation parameters for both models are given in figures 20 and 21. In both models $(q_{\text{in}}, q_{\text{on}}) = (1964, 600)$ vehicles/h.

The OMJ upstream of the on-ramp shows the same features as on a homogeneous road without on-ramp as mentioned above. The random emergence and dissolution of narrow moving jams on a short time scale, which is characteristic for OMJ (figures 21 (figures right) and 22 (figures right)), is qualitatively different from the behaviour inside the widening synchronized flow pattern (WSP), which occurs spontaneously at the same parameters in the KKW models within the three-phase traffic theory (figures 21 (figures left) and 22 (figures left)).

Indeed, whereas inside WSP in the KKW models vehicles can move with nearly constant vehicle speed (figures 21(*b*) and 22(*b*)), in the NaSch CA model with comfortable driving inside OMJ the vehicles must randomly slow down sharply sometimes up to a stop and then accelerate within a short time scale, and so on (figures 21(*e*) and 22(*d*)). The inverse distance between vehicles shows the same high amplitude oscillating behaviour inside OMJ in the NaSch CA model with comfortable driving (figure 21(*f*)). Its amplitude is much higher than would be expected due to bare model fluctuations. This is the result of non-linear amplification

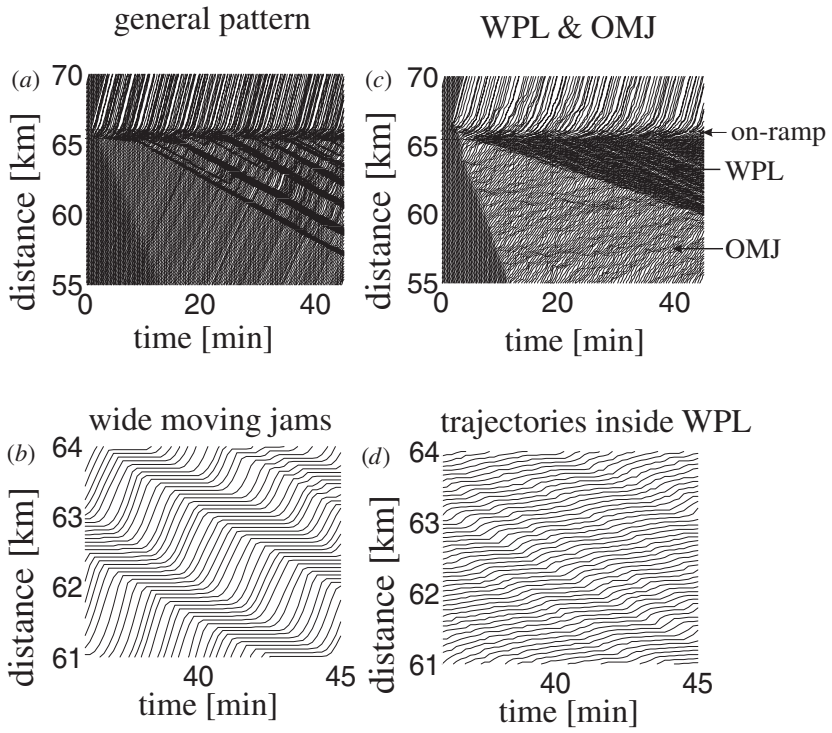

Figure 24. Comparison of the vehicle trajectories related to the patterns in figure 23: GP in the KKW-1 model (table 1) (figures left), congested pattern at the on-ramp in the NaSch CA model with comfortable driving (figures right). Model specifications as in figures 20 and 21. (*a*) Vehicle trajectories (overview) of GP shown in figure 23(*a*). (*b*) Vehicle trajectories inside the region of wide moving jams in GP. (*c*) Vehicle trajectories (overview) of WPL and further upstream OMJ corresponding to figure 23(*d*). (*d*) Vehicle trajectories inside WPL. Only trajectories of every 7th vehicle are shown.

of fluctuations in the NaSch CA model with comfortable driving. In contrast, in the KKW models the inverse distance between vehicles shows only small changes in WSP, the amplitude of which is comparable to the bare model fluctuations. Thus, WSP in our CA models within the three-phase traffic theory has a qualitatively different nature in comparison with OMJ in the NaSch CA model with comfortable driving.

(iii) If the flow rate q_{on} is further gradually increasing first no transition to another congested traffic pattern occurs in the NaSch CA model with comfortable driving: OMJ persists in some range of the flow rate q_{on} (the region between the boundaries O and L which is marked 'OMJ' in the diagram of congested patterns in figure 20).

(iv) However, above some flow rate q_{on} a widening region of very low mean vehicle speed (about $v = 10$ km h^{-1}) and very low mean flow rate ($q_{\text{LP}} \approx 480$ vehicles/h) occurs spontaneously upstream of the on-ramp in the NaSch CA model with comfortable driving (figures 23(*d*)–(*f*) and figures 24(*c*) and (*d*)).

The downstream front of this congested pattern is pinned at the on-ramp and the upstream front is slowly moving upstream. Therefore, this pattern may be called 'the widening pinned layer' (WPL for short). Inside WPL as well as in OMJ, a very complex non-stationary behaviour of vehicles occurs. This random behaviour resembles that in OMJ, however with two differences: (1) the maximal vehicle speed in WPL is much lower than in OMJ, and

(2) the vehicles come much more frequently to a stop in WPL. Because of the extremely low mean vehicle speed and large fluctuations in WPL, we cannot discern a regular pattern in WPL. States in which vehicles stop can emerge and dissolve stochastically but in a correlated way at different locations in WPL with time scale of about 5–10 min. These correlations in WPL seem to propagate with a velocity faster than the propagation of the front between WPL and OMJ.

(v) If the whole range of the flow rates $q_{\rm in}$ on the road upstream of the on-ramp and the flow rate $q_{\rm on}$ to the on-ramp is studied, then the conclusion can be drawn that there are only two different congested patterns in the NaSch CA model with comfortable driving at the on-ramp: the pinned layer (PL) which can be either widening (WPL) or localized (LPL) and OMJ. In addition, a combination of WPL and OMJ is possible (the latter pattern is marked as 'WPL & OMJ' in figures 23(d)–(f) and 24(c)).

In particular, if the flow rate $q_{\rm in} \geqslant q_{\rm OMJ}$ (at $q_{\rm in} = q_{\rm OMJ}$ the boundaries O and L intersect one another), then to the right of the boundary L in the diagram of patterns for the NaSch CA model with comfortable driving WPL occurs at the on-ramp, and upstream of this widening pinned layer OMJ is realized (in the region marked as 'WPL & OMJ' in figure 20). The case of such a spatial combination of WPL and OMJ is shown in figures 23(d)–(f) and 24(c)).

The same combination of WPL and OMJ occurs spontaneously from an initial state of free flow, if the flow rate $q_{\rm in}$ is within the range $q_{\rm W} < q_{\rm in} \leqslant q_{\rm OMJ}$. This occurs, when the flow rate to the on-ramp $q_{\rm on}$ is increasing and becomes larger than that which is related to the boundary O.

However, if the flow rate $q_{\rm in}$ is within the range $q_{\rm PL} < q_{\rm in} \leqslant q_{\rm W}$, then no OMJ occurs upstream of the WPL right of the boundary O (the region marked 'WPL' in the diagram of congested patterns in figure 20). In the latter case, free flow is realized upstream of the WPL.

If the flow rate $q_{\rm in} < q_{\rm PL}$, then right of the boundary O the pinned layer occurs whose upstream front does not move continuously upstream. Indeed, in this case the flow rate $q_{\rm in}$ upstream of the pinned layer is lower than the mean flow rate inside the pinned layer $q_{\rm PL}$. This means that the localized pinned layer (LPL) rather than WPL occurs in the region marked 'LPL' in the diagram in figure 20. The vehicle behaviour inside LPL is qualitatively the same as inside WPL. Note that OMJ and WPL, and also LPL, which occur in the NaSch CA model with comfortable driving at the on-ramp, have *not* been observed in empirical observations [8].

These congested patterns in the NaSch CA model with comfortable driving are qualitatively different from those which occur spontaneously for the same conditions in the KKW models within three-phase traffic theory (table 1). These differences are summarized below.

(1) At the same given flow rate on the one-lane road upstream of the on-ramp, $q_{\rm in}$, and at some flow rate $q_{\rm on}$, where OMJ is formed in the NaSch CA model with comfortable driving, WSP occurs spontaneously upstream of the on-ramp in the KKW models. It can be seen from figures 21(a)–(c) and figures 22(a) and (b), where the spatial vehicle speed distribution in the WSP is shown, that these pattern characteristics are different from OMJ shown in figures 21(d)–(f) and figures 22(c) and (d). In particular, whereas OMJ in the NaSch CA model with comfortable driving is characterized by a complex birth and decay of narrow moving jams, no moving jams were seen in WSP.

(2) If the flow rate $q_{\rm on}$ is further gradually increasing, WSP spontaneously transforms either into DGP or into GP in our CA models within three-phase traffic theory. At high flow rate to the on-ramp $q_{\rm on}$ the GP does not transform into any other kind of congested pattern: the GP remains GP no matter how high the flow rate $q_{\rm on}$ upstream of the on-ramp is. In contrast, if the flow rate to the on-ramp $q_{\rm on}$ increases for a given value $q_{\rm in} > q_{\rm OMJ}$ in the

NaSch CA model with comfortable driving, then to the right of the boundary L in figure 20 a WPL develops upstream of the on-ramp.

(3) In the NaSch CA model with comfortable driving upstream of WPL the oscillating moving jams (OMJ) occur spontaneously, if $q_{\text{in}} > q_{\text{OMJ}}$ (figures 20 and 23(d)). In the KKW models within three-phase traffic theory, however, upstream of the most upstream wide moving jam in the GP a region of synchronized flow is realized, where no oscillations and no moving jams occur (figure 23(a)).

(4) In the pinch region of the GP in our CA models within three-phase traffic theory narrow moving jams emerge. Some of these narrow moving jams grow and transform into wide moving jams spontaneously at the upstream front of the pinch region (figures 8(a) and (b) and figure 7(a)). These wide moving jams propagate further upstream without any limitation. Thus, in the KKW models wide moving jams which possess the characteristic parameters mentioned above (section 5.1) *spontaneously* occur in GP. In contrast, in the NaSch CA model with comfortable driving narrow moving jams do not transform into wide moving jams. Instead, OMJ or WPL patterns are formed. In other words, in contrast to our CA models within three-phase traffic theory, in the NaSch CA model with comfortable driving *no spontaneous* emergence of wide moving jams which possess the characteristic parameters mentioned above (section 5.1) occurs: in their model, such a wide moving jam can only be excited by an additional external perturbation of a very large amplitude (which was done in [23] in order to create the wide moving jam), i.e. by a perturbation which forces one of the vehicles to stop for several time steps.

(5) The fact that no wide moving jams can *spontaneously* occur in the NaSch CA model with comfortable driving can be seen from a comparison of the left pictures for GP with the right pictures for WPL in figures 23 and 24. In particular, there is a clear regular spatiotemporal structure of wide moving jams which alternate with the regions where vehicles move sometimes with nearly the maximal vehicle speed inside GP (left figures), whereas there is no such region inside WPL (right figures).

Moreover, wide moving jams which have spontaneously occurred in GP (figures 23(a) and 24(a)) propagate further without any limitation upstream. In contrast, in the NaSch CA model with comfortable driving regions inside WPL, where vehicles come to a stop, can emerge and dissolve randomly during several minutes. These regions do *not* propagate through the upstream boundary of WPL.

5.3. Conclusions about features of the KKW models in the three-phase traffic theory

Several CA models belonging to three-phase traffic theory were proposed in this paper. Their simulation gives results that allow us to draw the following conclusions.

(i) The conditions (1), (3) from [24], where due to the introduction of the synchronization distance D a 2D region of the steady states in the flow density plane appears, allow the formulation of *several different sets of specific functions* for fluctuations and for the vehicle acceleration and deceleration which lead to *qualitatively the same diagram of congested patterns* at on-ramps.

(ii) In the KKW model formulation, specific functions for fluctuations and for the vehicle acceleration and deceleration in the basic model (1), (3) can be much simpler than in [24]. Nevertheless, the main features of the diagrams of congested patterns are qualitatively the same as within the three-phase traffic theory in [8, 24].

(iii) The diagrams of congested patterns in the KKW models within three-phase traffic theory have the following features which differ from the case considered in [24]. First, there is

no region in the diagrams of patterns where the moving synchronized flow pattern (MSP) occurs exclusively. However, MSP can spontaneously randomly emerge in the region 'WSP', where the widening synchronized flow pattern (WSP) occurs. Second, when the initial flow rate on the road upstream of the on-ramp $q_{\rm in}$ is higher than the mean flow rate in the wide moving jam outflow then the general pattern (GP) occurs at lower flow rates to the on-ramp in comparison with the case of the model in [24].

(iv) The congested patterns and the diagram of these patterns of the KKW models explain empirical pattern features [8] and their evolution, when the flow rate to the on-ramp is changing.

(v) Both the diagrams of congested patterns and the pattern features of the KKW models, which belong to three-phase traffic theory, are qualitatively different from those derived by Helbing *et al* for a wide class of traffic flow models in the fundamental diagram approach (for more details see [24]).

(vi) The features of congested patterns, which occur upstream of the on-ramp in the KKW models differ from those in NaSch CA models, which belong to the fundamental diagram approach, including that with comfortable driving (see section 5.2). This is due to qualitatively different rules of vehicle motion of the basic model (1), (3) [24] in the three-phase traffic theory in comparison with NaSch CA models [1, 2, 22, 23, 36–40, 47, 49].

Acknowledgments

We would like to thank Kai Nagel for useful comments. BSK acknowledges funding by BMBF within project DAISY.

References

[1] Helbing D 2001 *Rev. Mod. Phys.* **73** 1067
[2] Chowdhury D, Santen L and Schadschneider A 2000 *Phys. Rep.* **329** 199
[3] Kerner B S 1999 *Phys. World* **12** 25
[4] Kerner B S 2001 *Netw. Spatial Econ.* **1** 35
[5] Kerner B S and Rehborn H 1996 *Phys. Rev.* E **53** R4275
[6] Kerner B S 1998 *Phys. Rev. Lett.* **81** 3797
[7] Kerner B S 2000 *Transp. Res. Rec.* **1710** 136
[8] Kerner B S 2002 *Phys. Rev.* E **65** 046138
[9] Kerner B S 2000 *J. Phys. A: Math. Gen.* **33** L221
[10] Helbing D, Hennecke A and Treiber M 1999 *Phys. Rev. Lett.* **82** 4360
[11] Lee H Y, Lee H W and Kim D 1998 *Phys. Rev. Lett.* **81** 1130
[12] Lee H Y, Lee H W and Kim D 1999 *Phys. Rev.* E **59** 5101
[13] Lee H Y, Lee H W and Kim D 2000 *Physica* A **281** 78
[14] Lee H Y, Lee H W and Kim D 2000 *Phys. Rev.* E **62** 4737
[15] Treiber M, Hennecke A and Helbing D 2000 *Phys. Rev.* E **62** 1805
[16] Treiber M and Helbing D 1999 *J. Phys. A: Math. Gen.* **32** L17–L23
[17] Helbing D and Treiber M 2002 *Preprint* trafficforum/02031301
[18] Tomer E, Safonov L and Havlin S 2000 *Phys. Rev. Lett.* **84** 382
[19] Lubashevsky I and Mahnke R 2000 *Phys. Rev.* E **62** 6082
[20] Lubashevsky I, Mahnke R, Wagner P and Kalenkov S 2002 *Phys. Rev.* E **66** 016117
[21] Nelson P 2000 *Phys. Rev.* E **61** R6052
[22] Knospe W, Santen L, Schadschneider A and Schreckenberg M 2000 *J. Phys. A: Math. Gen.* **33** L477
[23] Knospe W, Santen L, Schadschneider A and Schreckenberg M 2002 *Phys. Rev.* E **65** 015101(R)
[24] Kerner B S and Klenov S L 2002 *J. Phys. A: Math. Gen.* **35** L31
[25] Rosswog S and Wagner P 2002 *Phys. Rev.* E **65**
[26] Fukui M, Nishinari K, Takahashi D and Ishibashi Y 2002 *Physica* A **303** 226–38
[27] May A D 1990 *Traffic Flow Fundamental* (Englewood Cliffs, NJ: Prentice-Hall)
[28] Lighthill M J and Whitham G B 1955 *Proc. R. Soc.* A **229** 317

[29] Gazis D C, Herman R and Rothery R W 1961 *Oper. Res.* **9** 545–67
[30] Newell G F 1961 *Oper. Res.* **9** 209
[31] Whitham G B 1990 *Proc. R. Soc.* A **428** 49
[32] Prigogine I 1961 *Theory of Traffic Flow* ed R Herman (Amsterdam: Elsevier) p 158
Prigogine I and Herman R 1971 *Kinetic Theory of Vehicular Traffic* (New York: Elsevier)
[33] Kerner B S and Konhäuser P 1994 *Phys. Rev.* E **50** 54–83
[34] Kerner B S, Konhäuser P and Schilke M 1995 *Phys. Rev.* E **51** 6243–6
[35] Herrmann M and Kerner B S 1998 *Physica* A **255** 163–88
[36] Nagel K 1993 *Physics Computing '92* ed R A de Groot and J Nadrchal (Singapore: World Scientific) p 419
Nagel K and Schreckenberg M 1992 *J. Physique* I **2** 2221
[37] Nagel K and Paczuski M 1995 *Phys. Rev.* E **51** 2909
[38] Schreckenberg M, Schadschneider A, Nagel K and Ito N *Phys. Rev.* E **51** 2939
[39] Barlovic R, Santen L, Schadschneider A and Schreckenberg M 1998 *Eur. J. Phys.* B **5** 793
[40] Wolf D E 1999 *Physica* A **263** 438
[41] Kerner B S 1998 *Proc. 3rd Symp. on Highway Capacity and Level of Service* vol 2 ed R Rysgaard (Denmark: Road Directorate, Ministry of Transport) pp 621–42
[42] Kerner B S 1999 *Transp. Res. Rec.* **1678** 160–7
[43] Kerner B S 1999 Transportation and traffic theory *Proc. 14th Int. Symp. on Transportation and Traffic Theory* ed A Ceder (Oxford: Elsevier) p 147
Kerner B S 2000 *Traffic and Granular Flow'99* ed D Helbing, H J Herrmann, M Schreckenberg and D E Wolf (Berlin: Springer) pp 253–83
[44] Koshi M, Iwasaki M and Ohkura I 1983 *Proc. 8th Int. Symp. on Transportation and Traffic Theory* ed V F Hurdle *et al* (Toronto, Ontario: University of Toronto Press) p 403
[45] Kerner B S 2002 *Preprints of the Transportation Research Board 81st Annual Meeting* TRB Paper 02-2918 (Washington DC: TRB)
Kerner B S 2002 *Trans. Res. Rec.* at press
Kerner B S 2002 *Transportation and Traffic Theory in the 21st Century* ed M A P Taylor (Amsterdam: Elsevier) pp 417–39
[46] Krauß S, Wagner P and Gawron C 1997 *Phys. Rev.* E **53** 5597
[47] Knospe W, Santen L, Schadschneider A and Schreckenberg M 2002 *Preprint* cond-mat/0202346
[48] Wiedemann R 1974 *Simulation des Straßenverkehrsflusses* Schriftenreihe des Instituts für Verkehrswesen der Universität Karlsruhe, Germany, Heft 8
[49] Nagel K, Wolf D E, Wagner P and Simon P 1998 *Phys. Rev.* E **58** 1425
[50] Brilon W and Wu H 1999 *Traffic and Mobility* ed W Brilon, F Huber, M Schreckenberg and H Wallentowitz (Berlin: Springer) pp 163–80
[51] Takayasu M and Takayasu H 1993 *Fractals* **1** 860
[52] Kerner B S 2002 *Traffic and Granular Flow'01* ed M Fukui, Y Sugiyama, M Schreckenberg and D Wolf (Berlin: Springer) at press
[53] Mahnke R and Pieret N 1997 *Phys. Rev.* E **56** 2666
[54] Mahnke R and Kaupužs J 1999 *Phys. Rev.* E **59** 117
[55] Kühne R, Mahnke R, Lubashevsky I and Kaupužs J 2002 *Phys. Rev.* E **66** 066125
[56] Jost D 2002 Breakdown and recovery in traffic flow models *Master's Thesis* ETH Zürich
[57] Jost D and Nagel K 2002 *Preprint* cond-mat/0208082
[58] Hall F L, Hurdle V F and Banks J H 1992 *Transp. Res. Rec.* **1365** 12–8
[59] Persaud B, Yagar S and Brownlee R 1998 *Transp. Res. Rec.* **1634** 64–9
[60] Kerner B S and Rehborn H 1996 *Phys. Rev.* E **53** R1297
[61] Bando M, Hasebe K, Nakayama A, Shibata A and Sugiyama Y 1995 *J. Physique* I **5** 1389
[62] Kerner B S 2002 *Math. Comput. Modelling* **35** 481–508